Supporting Information

Water-soluble cyclometalated platinum(II) and iridium(III) complexes: synthesis, tuning of the photophysical properties, and *in vitro* and *in vivo* phosphorescence lifetime imaging.

Anastasia I. Solomatina, Shih-Hao Su, Maria M. Lukina, Varvara V. Dudenkova, Vladislav I. Shcheslavskiy, Cheng-Ham Wu, Pavel S. Chelushkin, Pi-Tai Chou*, Igor O. Koshevoy, Sergey P. Tunik*

Section 1. Synthesis of platinum and iridium complexes

Cyclometallating N^CH ligands, 2-phinylpiridine and methyl 2-phenylquinoline-4-carboxylate, were purchased from Sigma-Aldrich (USA), 2-(benzofuran-3-yl)pyridine and 2-(benzothiophen-3-yl)pyridine were obtained according Suzuki reaction [1,2]. Sulfonated diphosphine, 1,2-Bis(di-4-sulfonatophenylphosphino)benzene tetrasodium salt (P^P*), was purchased from Strem Chemicals (USA). Cyclometalated platinum(II) and iridium(III) complexes containing hydrophobic and water soluble diphosphines were obtained in good yield using slightly modified conventional procedures (Scheme 1 in main text of the article). In the case of platinum complexes, the synthesis started from the reaction of K_2PtCl_4 with 2-fold excess of the corresponding N^CH precursor in 2-ethoxyethanol/water 7:4 at 85°C. For better solubility of the reactants, the chloro-bridged platinum dimer was converted into the mononuclear DMSO-substituted complex by heating in DMSO at 80ºC for 24 h. The final products were obtained in the reaction of DMSO complex with the corresponding phosphine either in CH_2Cl_2 or in the CH_2Cl_2/MeOH mixture depending on the hydrophilicity of the P^P-ligand. Cationic platinum complexes with 1,2-bis(diphenylphosphino)benzene (dppb) were obtained in good yield (90-98%) in dichloromethane solution at room temperature according to published protocol [3]. The final products were crystallized from dichloromethane/hexane system at +4 °C. Water-soluble complexes were obtained by mixing of methanol solution of the sulfonated P^P* ligand and dichloromethane solution of the cyclometalating precursor. Note that this phosphine readily oxidizes and even commercially available substance contains a few percent of phosphine oxide that lowers the yield of reaction (65-85%) and necessitates additional product purification to separate unreactive phosphine oxide, see Experimental Section for details. Water-soluble iridium complexes were obtained through the reaction of equimolar amount $IrCl_3*6H_2O$ and orthometalating ligand precursor (N^CH) in 2-ethoxyethanol/water 7:4 at 100°C, followed by treatment of the chloro-bridged iridium dimers with the sulfonated phosphine.

Synthesis of platinum complexes with sulfonated phosphine

Complex Pt1*. [ppyPt(DMSO)Cl] (20 mg, 0.0432 mmol) was dissolved in ca. 3 ml of degassed CH_2Cl_2 and diphosphine (48 mg, 0.053 mmol) was dissolved in ca. 3 ml of degassed MeOH.

Solutions were mixed up and stirred for 1 h under nitrogen. Then precipitate were collected, washed with a mixture of a dichloromethane/methanol 1:1 ca. 3 ml, and dried under vacuum. Yield of pale-green solid – 43 mg, 84%. ^{1}H NMR (400 MHz, CD_3OD, 298 K): δ 8.46 (m with broad ^{195}Pt satellites, 1H[1]), 8.17 (d, $^{3}J_{H-H}$ = 8.2 Hz, 1H[4]), 8.09 – 7.85 (m, 19H), 7.81 – 7.71 (m, 3H), 7.23 (m with broad ^{195}Pt satellites, 1H[8]), 7.17 (t, J = 7.6 Hz, 1H[2]), 7.13 (d, $^{3}J_{H-H}$ = 6.7 Hz, 1H[6]), 6.90 (t, $^{3}J_{H-H}$ = 7.5 Hz, 1H[7]) ppm. ^{31}P NMR (162 MHz, CD_3OD, 298 K): δ 48.51 (d, $^{1}J_{P-Pt}$ = 1802 Hz), 36.70 (d, $^{1}J_{P-Pt}$ = 3766 Hz) ppm. ES MS (*m/z*): $[M-3Na]^{3-}$ 370.658 (calc. 370.655), $[M-2Na]^{2-}$ 567.482 (calc. 567.477), $[2M-3Na]^{3-}$ 763.971 (calc. 763.965), $[M-Na]^{-}$ 1157.954 (calc. 1157.942).

Complex Pt2*. btpyPt(DMSO)Cl (30 mg, 0.058 mmol) was dissolved in ca. 5 ml of degassed CH_2Cl_2 and diphosphine (63 mg, 0.070 mmol) was dissolved in ca. 5 ml of degassed MeOH. Solutions were mixed up and stirred for 1 h under nitrogen. Then solvent was removed under vacuum and product was precipitated from concentrated methanol. The precipitate was centrifuged and washed with small portions of MeOH (ca. 3 x 0.5 ml) to remove phosphineoxide. Yield of pale-yellow amorphous solid – 55 mg, 77 %. ^{1}H NMR (400 MHz, CD_3OD, 298 K): δ 8.39 (m, with broad ^{195}Pt satellites, 1H[1]), 8.33 (d, $^{3}J_{H-H}$ = 8.2 Hz, 1H[4]), 8.27 (d, $^{3}J_{H-H}$ = 8.4 Hz, 1H[5]), 8.12 (t, $^{3}J_{H-H}$ = 7.2 Hz, 1H[3]), 8.01 (dd, $^{3}J_{H-H}$ = 9.7, 3.9 Hz, 18H[10-12]), 7.78 (m, 2H[9]), 7.70 (d, $^{3}J_{H-H}$ = 8.1 Hz, 1H[8]), 7.44 (t, $^{3}J_{H-H}$ = 7.3 Hz, 1H[6]), 7.27 (t, $^{3}J_{H-H}$ = 7.6 Hz, 1H[7]), 7.06 (t, $^{3}J_{H-H}$ = 6.6 Hz, 1H[2]) ppm. ^{31}P NMR (162 MHz, CD_3OD, 298 K): δ 48.60 (d, $^{1}J_{P-Pt}$ = 2140 Hz), 32.72 (d, $^{1}J_{P-Pt}$ = 3463 Hz) ppm. ES MS (*m/z*): $[M-3Na]^{3-}$ 389.315 (calc. 389.312), $[M-2Na]^{2-}$ 595.470 (calc. 595.463), $[2M-3Na]^{3-}$ 801.290 (calc. 801.280), $[M-Na]^{-}$ 1213.929 (calc. 1213.914).

Complex Pt3*. Complex was obtained as compound **Pt2***. Yield of pale-yellow amorphous solid – 75 %. ^{1}H NMR (400 MHz, CD_3OD, 298 K): δ 8.28 (m, with broad ^{195}Pt satellites, 1H[1]), 8.08 (t, $^{3}J_{H-H}$ = 8.0 Hz, 1H[3]), 7.98 (m, 19H[4, 10-12]), 7.84 (d, $^{3}J_{H-H}$ = 7.6 Hz, 1H[5]), 7.84 – 7.78 (m, 2H[9]), 7.34 – 7.17 (m, 3H[6,8,7]), 7.07 (m, 1H[2]) ppm. ^{31}P NMR (162 MHz, CD_3OD, 298 K): δ 48.84 (d, $^{1}J_{P-Pt}$ = 2154 Hz), 34.08 (d, $^{1}J_{P-Pt}$ = 3496 Hz) ppm. ES MS (*m/z*): $[M-3Na]^{3-}$ 383.988 (calc. 383.986), $[M-2Na]^{2-}$ 587.479 (calc. 587.474), $[2M-3Na]^{3-}$ 790.628 (calc. 790.628), $[M-Na]^{-}$ 1197.946 (calc. 1197.937).

Complex Pt4*. [qpyPt(DMSO)Cl] (30 mg, 0.053 mmol) was dissolved in ca. 5 ml of degassed CH_2Cl_2 and diphosphine (58 mg, 0.064 mmol) was dissolved in ca. 5 ml of degassed methanol. Solutions were mixed and stirred for 1 h under nitrogen. Then solvent was removed under vacuum and the substance was dissolved in ca. 1 ml of methanol. The product was recrystallized during evaporation of the solvent. Yield of orange glass – 48 mg, 70 %. ^{1}H NMR (400 MHz, CD_3OD, 298 K): δ 8.53 (d, $^{3}J_{H-H}$ = 8.5 Hz, 1H[6]), 8.45 (s, 1H[5]), 8.29 (d, $^{3}J_{H-H}$ = 8.6 Hz, 1H[9]), 8.03 (m, 4H[12]), 7.92 (m, 4H[13]), 7.85 (d, $^{3}J_{H-H}$ = 7.7 Hz, 1H[4]), 7.73 (m, 4H[12']), 7.71 – 7.55 (m, 4H[10-11]), 7.52 (t, $^{3}J_{H-H}$ = 8.2 Hz, 1H[7]), 7.47 (m, 4H[13']), 7.20 – 7.15 (m with broad ^{195}Pt satellites, 1H), 7.13 (t, $^{3}J_{H-H}$ =

7.5 Hz, 1H), 6.98 (ddd, $^{3}J_{H\text{-}H}$ = 8.4, 7.1, $^{4}J_{H\text{-}H}$ = 1.2 Hz, 1H), 6.86 (t, $^{3}J_{H\text{-}H}$ = 7.4 Hz, 1H), 2.17 (s, 4H^{14}) ppm. ^{31}P NMR (162 MHz, CD_3OD, 298 K): δ 43.48 (d, $^{1}J_{P\text{-}Pt}$ = 1755 Hz), 36.35 (d, $^{1}J_{P\text{-}Pt}$ = 3879 Hz) ppm. ES MS (*m/z*): $[M\text{-}3Na]^{3-}$ 406.678 (calc. 406.662), $[M\text{-}3Na+H]^{2-}$ 610.519 (calc. 610.496), $[M\text{-}2Na]^{2-}$ 621.511 (calc. 621.487).

The molecular structures of the cationic [Pt(N^C)(P^P)]PF_6 platinum complexes containing non-sulfonated diphosphine (**Pt1**, **Pt2**, **Pt4)** in crystal state were estimated by the XRD analysis (Fig. S1, Table S1) and used as reference data for elucidation of the structure of sulfonated analogues. The square-planar motifs of these compounds are essentially similar and include two bidentate ligands (N^C and P^P), both of which chelate the metal center and thus saturating its coordination sphere. The principal structural parameters for **Pt1**, **Pt2**, **Pt4** (selected interatomic distances and bond angles are listed in Table S2) are comparable to the corresponding values determined for the congener cationic diphosphine species [3,4]. The clearly visible deviation of the Pt–P bond lengths, which are systematically longer for the phosphorus atoms in *trans* positions to carbanions (2.298–2.327 Å *vs* 2.231–2.247 Å for P–Pt *trans* to N atoms), matches earlier observations and are attributed to the different electron-donating ability of C^- and N sites of the cyclometalated ligands. In the case of **Pt1** and **Pt2** compounds, the ligand environments do not induce substantial steric hindrance. The N^C fragments lie approximately in one plane with the diphosphine phenylene backbone that is reflected by small angles between the planes defined by the metalated aromatic systems and $\{P_2C_6H_4\}$ motifs, which amount to 8.1–9.2° and 7.7° for **Pt1** and **Pt2**, respectively.

On the contrary, complex **Pt4** with bulkier quinoline moiety reveals severe structural distortions due to the repulsion between the protons of the rigid N^C ligand (*ortho* to the P atom) and the phenyl rings of dppb, though the bond distances around the metal center remain unexceptional. Thus, the phenyl-quinoline part of the molecule displays considerable bending, which is enhanced by the displacement of platinum center that forms a non-planar five-membered metallocycle. Alike features are found for the diphosphine ligand, the phenylene ring of which is twisted with respect to the phosphorus atoms and pushed out of the P–Pt–P plane to keep the pseudo-tetrahedral geometry of the P donors. Ultimately, minimization of the unfavorable intramolecular contacts leads to a large angle between the plane defined by the NCCC atoms of the metalated ring and that of the diphosphine backbone (64.1°).

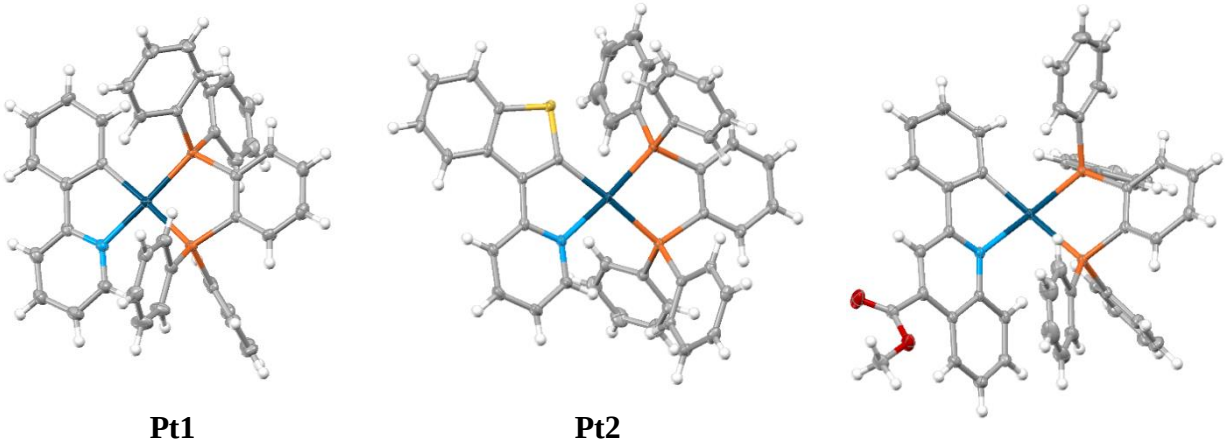

Pt1 **Pt2** **Pt4**

Figure S1. Molecular structures of the **Pt1, Pt2, Pt4** complexes.

The presence of spatially voluminous diphosphines in complexes **Pt1**, **Pt2**, **Pt4** might account for the lack of intermolecular metal–metal bonding, frequently observed for platinum(II) species [5]. On the other hand, π-π stacking interactions, which involve the N^C ligands of the neighbouring head-to-tail arranged cations, are found for these structurally characterized compounds, Fig. S2.

Pt1

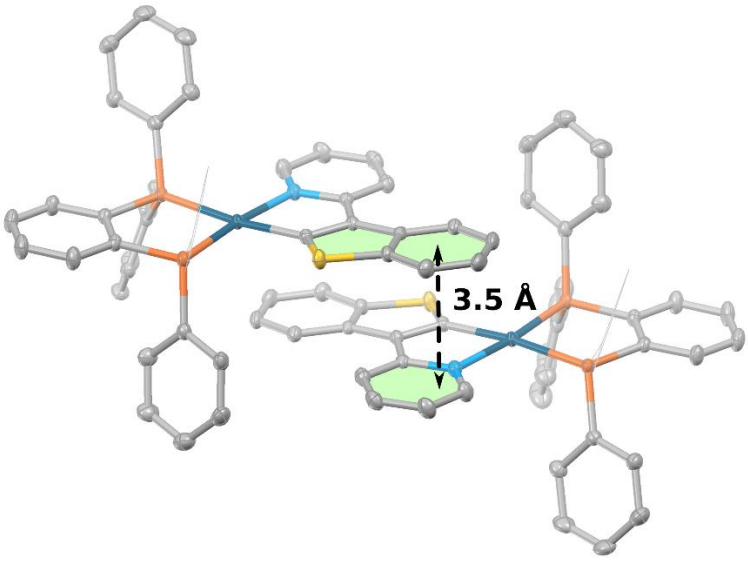

Pt2

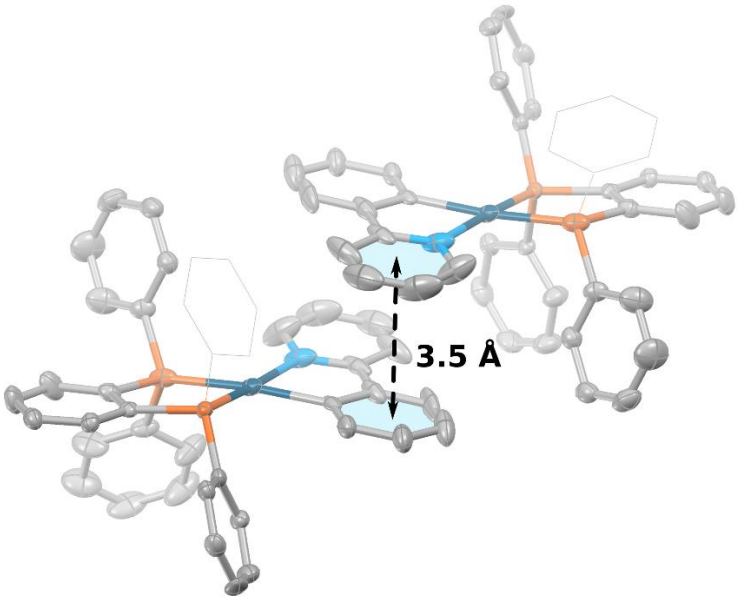

Pt4

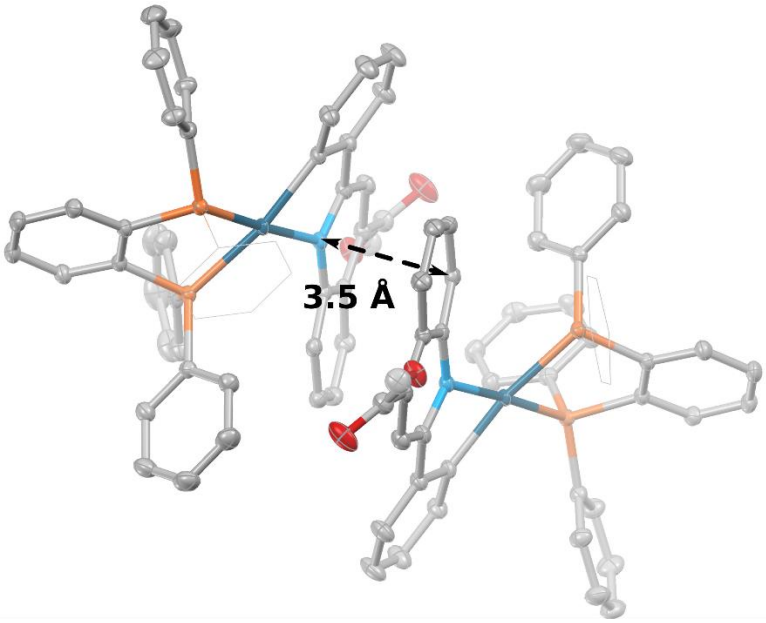

Figure S2. View of the packing diagram for **Pt1**, **Pt2** and **Pt4**. Thermal ellipsoids are shown at 50% probability level.

It is worth noting that structural analogues of the **Ir1*** and **Ir2*** complexes containing the non-sulfonated dppb have been synthesized earlier [6,7] and their structural patterns serve as a model for interpretation of the NMR spectroscopic data (Fig. S29-S32).

In solution, all compounds obtained were characterized using the ^{31}P, ^{1}H and ^{1}H-^{1}H COSY NMR spectroscopy and ESI mass-spectrometry (see Experimental and Figs. S3-S32). The ESI^{+} mass spectra of **Pt1**–**Pt4** reveal cations of the singly charged molecular ions (Figs S19-S22), whereas the ESI^{-} spectra of sulfonated **Pt1***–**Pt4*** complexes show the major signals corresponding to double and triple charged ions resulted from sodium ions dissociation from the $–SO_3Na$ moiety of the diphosphine (Figs. S23-S26). The ESI^{-} mass spectra of iridium complexes containing

sulfonated phosphine analogously show the set of signals corresponding to dissociation of sodium cations from the starting $[Ir(N\hat{}C)_2(P\hat{}P^*)]^+$ molecular ion (Figs. S21-S32). Thus, the mass-spectra of all complexes studied are completely compatible with the proposed composition and supplement the XRD and NMR data.

The platinum complexes have two inequivalent phosphine atoms, which display significantly different chemical shifts and Pt-P coupling constants in the ^{31}P NMR spectra ($\delta^A \approx 45$ ppm, $J_{P\text{-}Pt} \approx 2000$ Hz and $\delta^B \approx 35$ ppm, $J_{P\text{-}Pt} \approx 3600$ Hz). The former resonance has to be assigned to the phosphorus atom in *trans*-positions to the carbon atom in the metalating C^N-ligand, whereas the latter associated with the phosphorus located in *trans*-positions to the nitrogen atom, as lower coupling constants and longer bond length are normally ascribed to the stronger *trans*-influence of the metalating carbon [4,8].

The ^1H-^1H COSY spectra of the **Pt1**-**Pt4** and **Pt1***-**Pt4*** complexes made possible to attribute all signals in these spectra, see Figs. S11-S18. The number of signals, their multiplicity and relative intensity fit completely the structural patterns shown in Fig. S1.

The NMR data obtained for both iridium complexes (Figs. S27-S30) are also completely compatible with the structural patterns revealed earlier for the complexes containing non-sulfonated dppb [6] ligand. The C_2 symmetry axis passes through the benzyl ring of diphosphine ligand and metal center making phosphorus atoms equivalent that gives one signal in the ^{31}P NMR spectrum, Figs. S27-28). The same symmetry element makes the C^N ligands equivalent to give in the proton spectrum only one set of signals corresponding to these moieties (see Figs. S29-S30). However, this octahedral structural pattern is relatively rigid that prevents dynamic scrambling of the phenyl rings in the diphosphine ligand, thus two sulfonated phenyls are inequivalent that results in two sets of the phenyl protons in the ^1H NMR spectrum, Figs. S29-S30.

Thus, the NMR data obtained for the compounds synthesized show that the structures revealed in solid state using XRD crystallography are retained in fluid media both in organic solvents and in aqueous solutions for the complexes containing non-sulfonated and sulfonated phosphines, respectively.

Table S1. Crystal data and structure refinement for complexes **Pt1**, **Pt2** and **Pt4**.

Identification code	**1**	**2**	**3**
Empirical formula	C43H34Cl2F3NO3P2PtS	C44H32F3NO3P2PtS2	C48H36F3NO5P2PtS
Formula weight	1029.70	1000.85	1052.87
Temperature (K)		150(2)	
Wavelength (Å)		0.71073	
Crystal system	Triclinic	Triclinic	Triclinic
Space group	P -1	P -1	P -1
Unit cell dimensions			
a (Å)	9.3598(13)	9.0795(3)	12.1407(3)
b (Å)	14.568(2)	14.0701(5)	12.2755(3)
c (Å)	29.931(4)	18.4070(6)	14.8967(4)
a (º)	97.237(5)	106.2530(10)	101.7930(10)
β (º)	93.441(5)	99.7900(10)	99.3060(10)
γ (º)	94.101(5)	102.2840(10)	101.6470(10)
Volume ($Å^3$)	4028.3(9)	2138.74(13)	2080.25(9)
Z	4	2	2
ρ_{calc} (Mg/m^3)	1.698	1.554	1.681
μ (mm^{-1})	3.803	3.505	3.563
F(000)	2032	988	1044
Crystal size (mm^3)	0.649 x 0.125 x 0.118	0.180 x 0.141 x 0.036	0.195 x 0.097 x 0.066
θ range for data collection (º)	0.687 to 25.999	1.188 to 29.999	1.429 to 29.999
Index ranges	-11<=h<=11, -17<=k<=17, -36<=l<=36	-12<=h<=12, -19<=k<=19, -25<=l<=25	-17<=h<=17, -17<=k<=17, -20<=l<=20
Reflections collected	128086	87409	98754
Independent reflections	15837 [R(int) = 0.0511]	12462 [R(int) = 0.0280]	12134 [R(int) = 0.0274]
Completeness to θ= 25.24º	100.0 %	100.0 %	100.0 %
Absorption correction	Semi-empirical from equivalents	Numerical	Semi-empirical from equivalents
Max. and min. transmission	0.662 and 0.192	0.884 and 0.571	0799 and 0.543
Data/ restrains/ parameters	15837 / 54 / 1034	12462 / 0 / 505	12134 / 157 / 557
GOOF on F^2	1.058	1.060	1.044
Final R indices [I>2σ(I)][a]	R1 = 0.0342, wR2 = 0.0728	R1 = 0.0200, wR2 = 0.0495	R1 = 0.0267, wR2 = 0.0693
R indices (all data)	R1 = 0.0425, wR2 = 0.0758	R1 = 0.0221, wR2 = 0.0501	R1 = 0.0292, wR2 = 0.0707

Largest diff. peak and hole (e.Å^{-3})	2.787 and -2.689	1.863 and -1.181	2.248 and -1.799

[a] $R_1 = \Sigma||F_o| - |F_c||/\Sigma|F_o|$; $wR2 = [\Sigma\,[w(F_o^2 - Fc^2)^2]/\,\Sigma[w(F_o^2)^2]]^{1/2}$

Table S2. Selected bond lengths (Å) and angles (deg.) for complexes **Pt1**, **Pt2** and **Pt4** (two values for **Pt1** correspond to the independent molecules found in the unit cell).

	Pt1	**Pt2**	**Pt4**
Bond lengths, Å			
C(1)–Pt(1)	2.071(4) 2.091(5)	2.041(2)	2.049(3)
N(1)–Pt(1)	2.095(4) 2.096(4)	2.105(2)	2.104(2)
P(1)–Pt(1)	2.298(1) 2.305(2)	2.3152(4)	2.3269(6)
P(2)–Pt(1)	2.247(1) 2.235(1)	2.2315(5)	2.2306(6)
Bond angles, º			
C(1)–Pt(1)–N(1)	80.0(2) 79.6(2)	78.21(7)	79.19(9)
P(1)–Pt(1)–P(2)	86.17(4) 85.40(4)	85.91(2)	83.65(2)
N(1)–Pt(1)–P(1)	97.7(1) 99.4(2)	99.29(4)	97.52(6)
C(1)–Pt(1)–P(1)	174.9(1) 173.9(1)	173.44(5)	166.09(8)
N(1)–Pt(1)–P(2)	175.2(1)	174.20(4)	176.74(6)

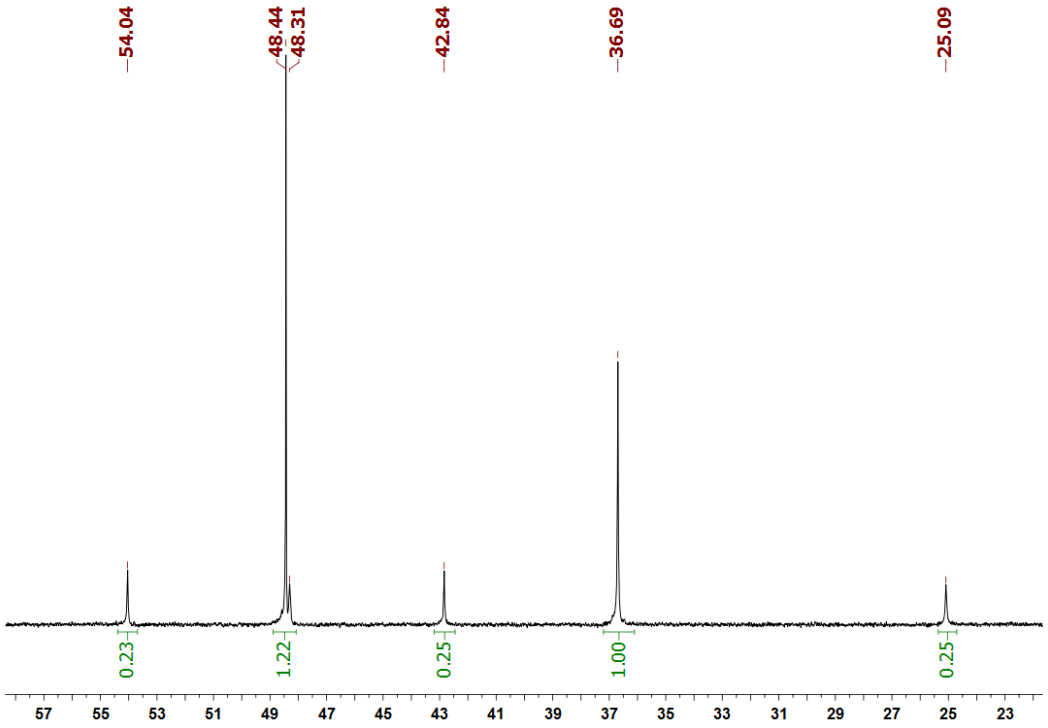

Figure S3. ^{31}P NMR spectrum of **Pt1**, CD3OD, 298K. CD_3OD, 298K.

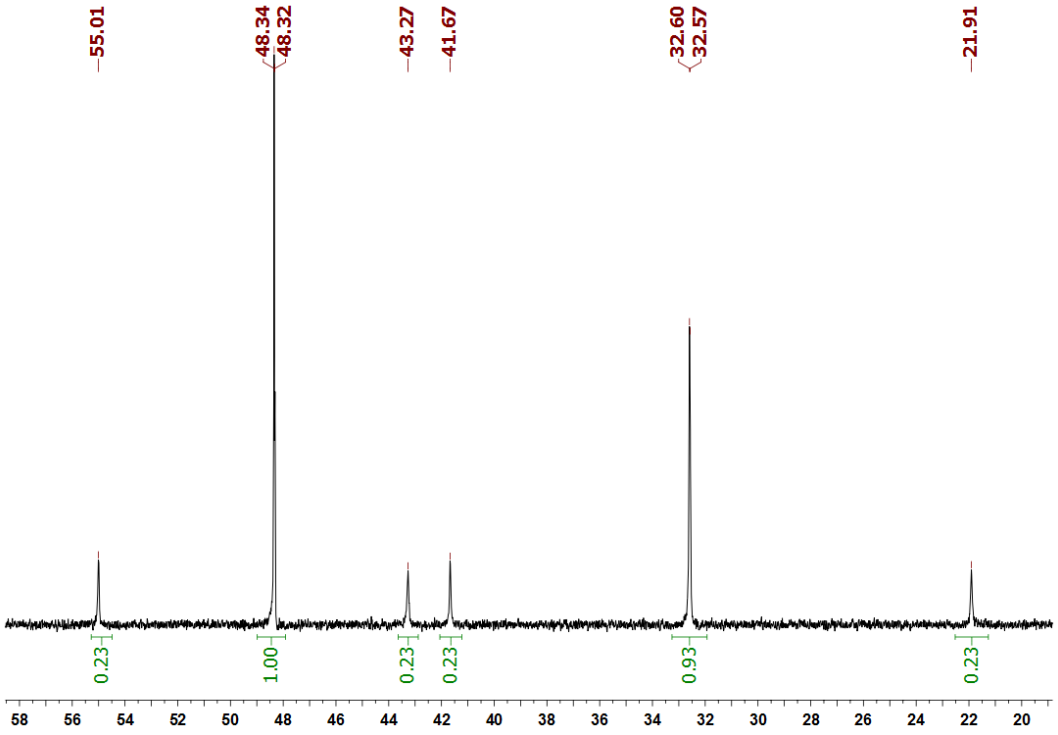

Figure S4. ^{31}P NMR spectrum of **Pt2**, CD_3OD, 298K.

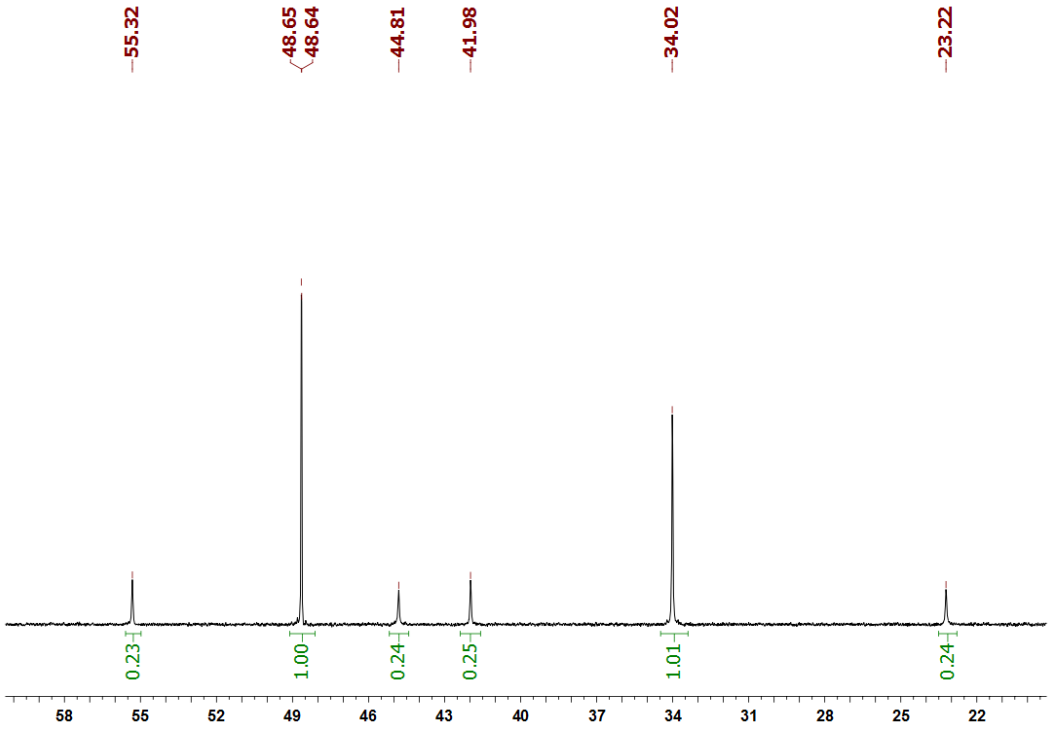

Figure S5. ^{31}P NMR spectrum of **Pt3**, CD_3OD, 298K.

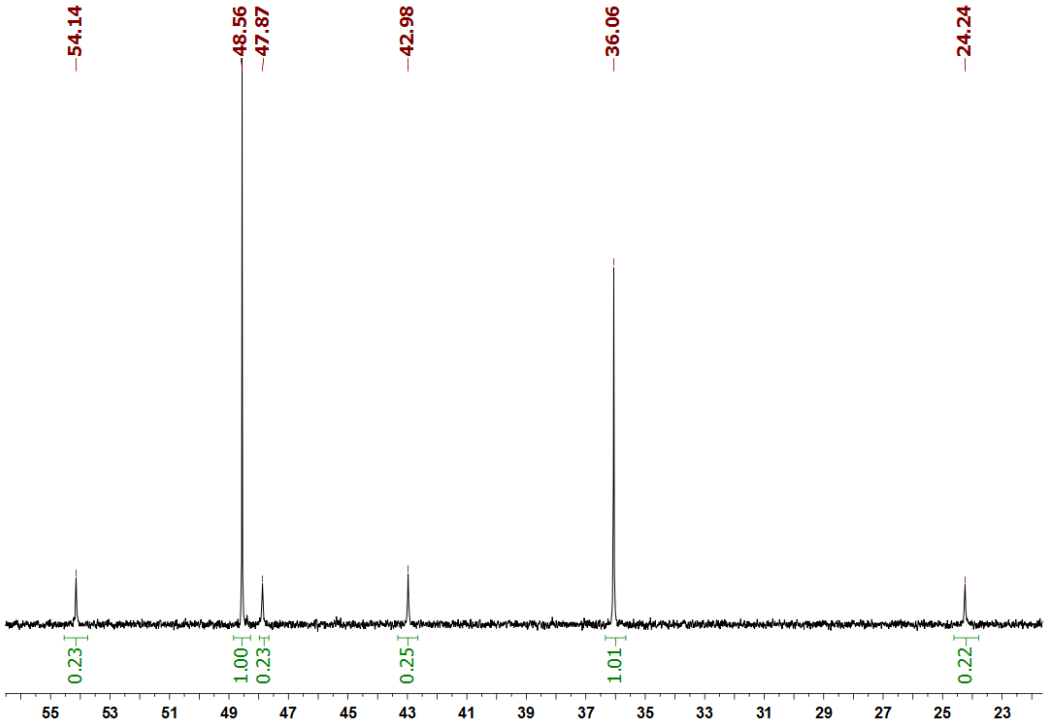

Figure S6. ^{31}P NMR spectrum of **Pt4**, CD_3OD, 298K.

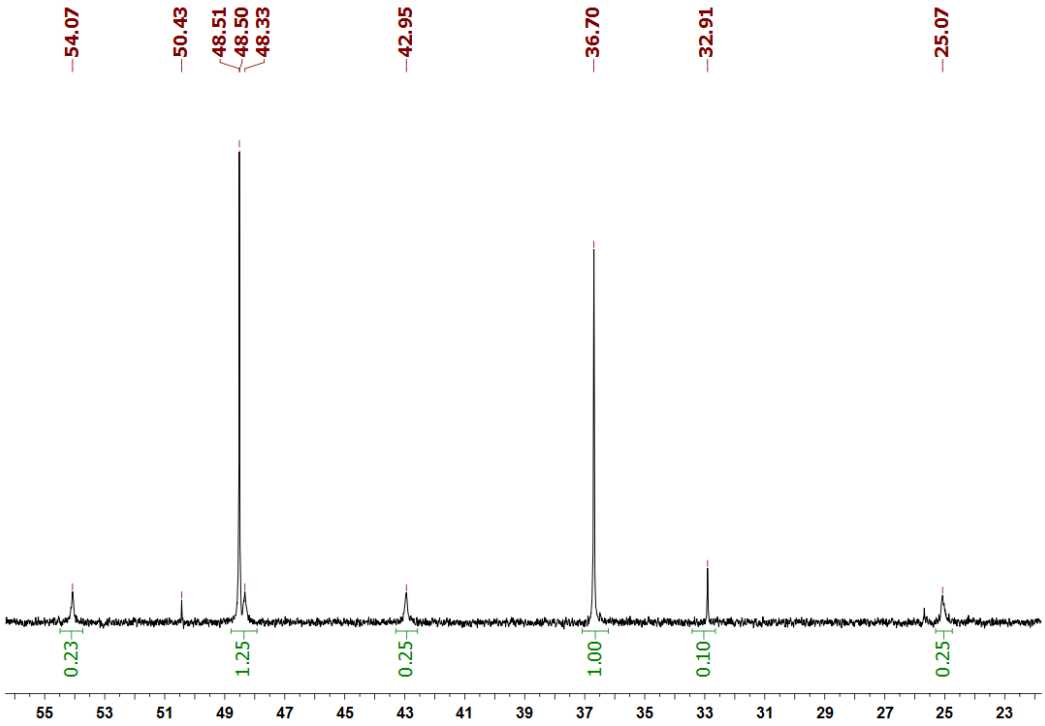

Figure S7. ^{31}P NMR spectrum of **Pt1***, CD_3OD, 298K.

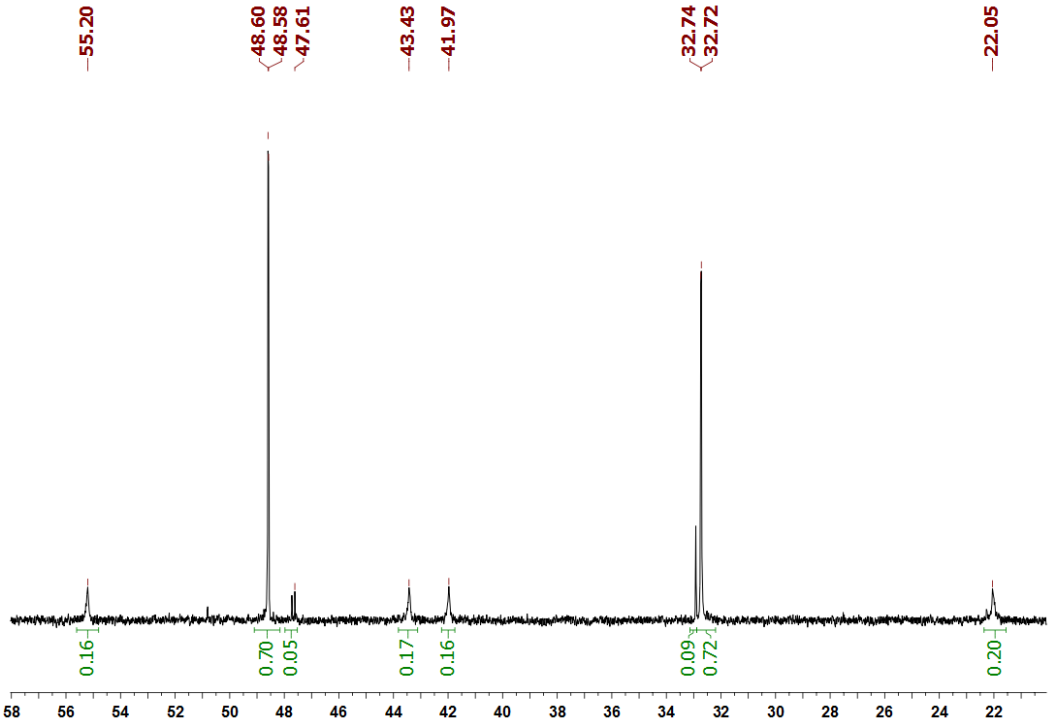

Figure S8. ^{31}P NMR spectrum of **Pt2***, CD_3OD, 298K.

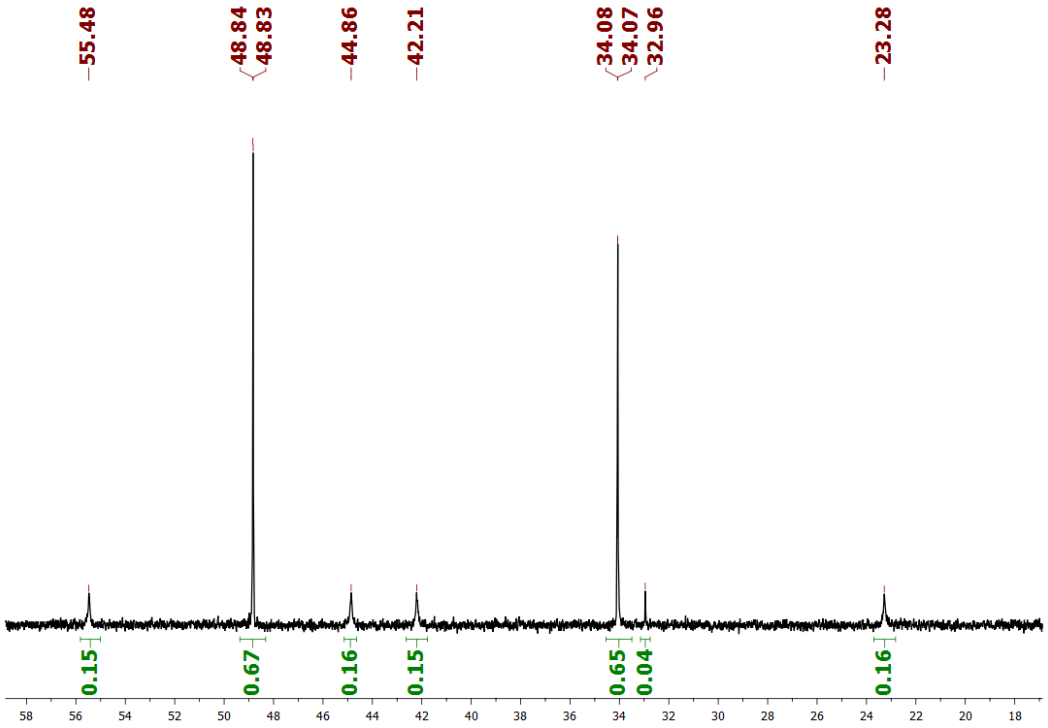

Figure S9. ^{31}P NMR spectrum of **Pt3***, CD_3OD, 298K.

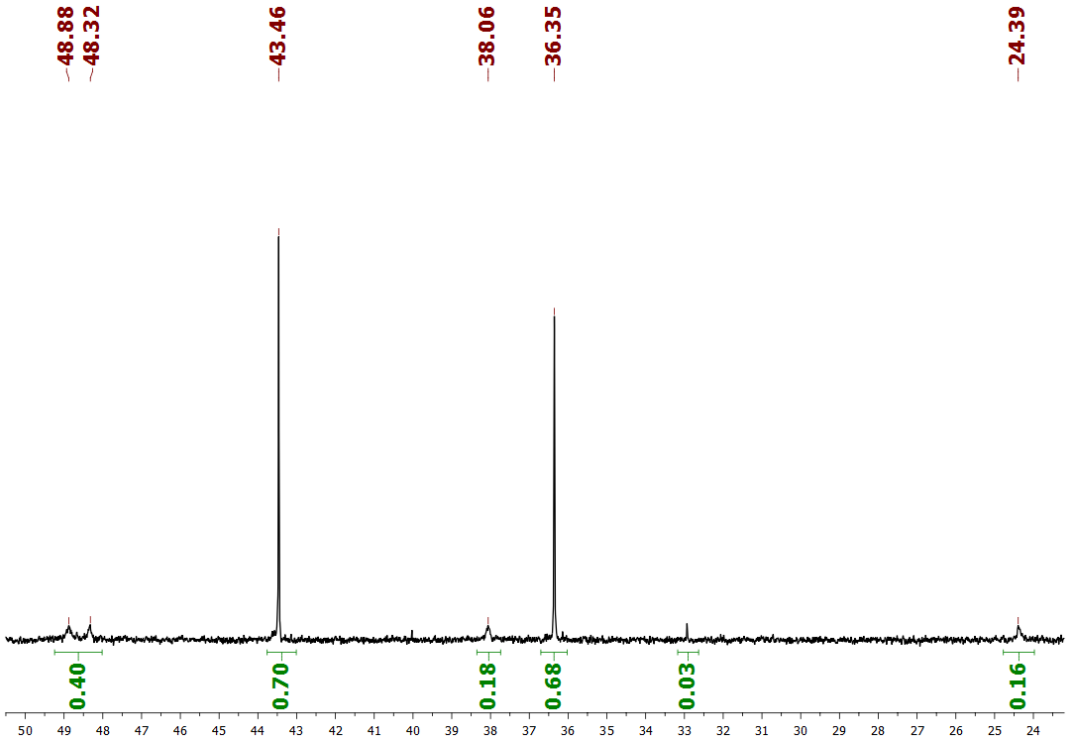

Figure S10. ^{31}P NMR spectrum of **Pt4***, CD_3OD, 298K.

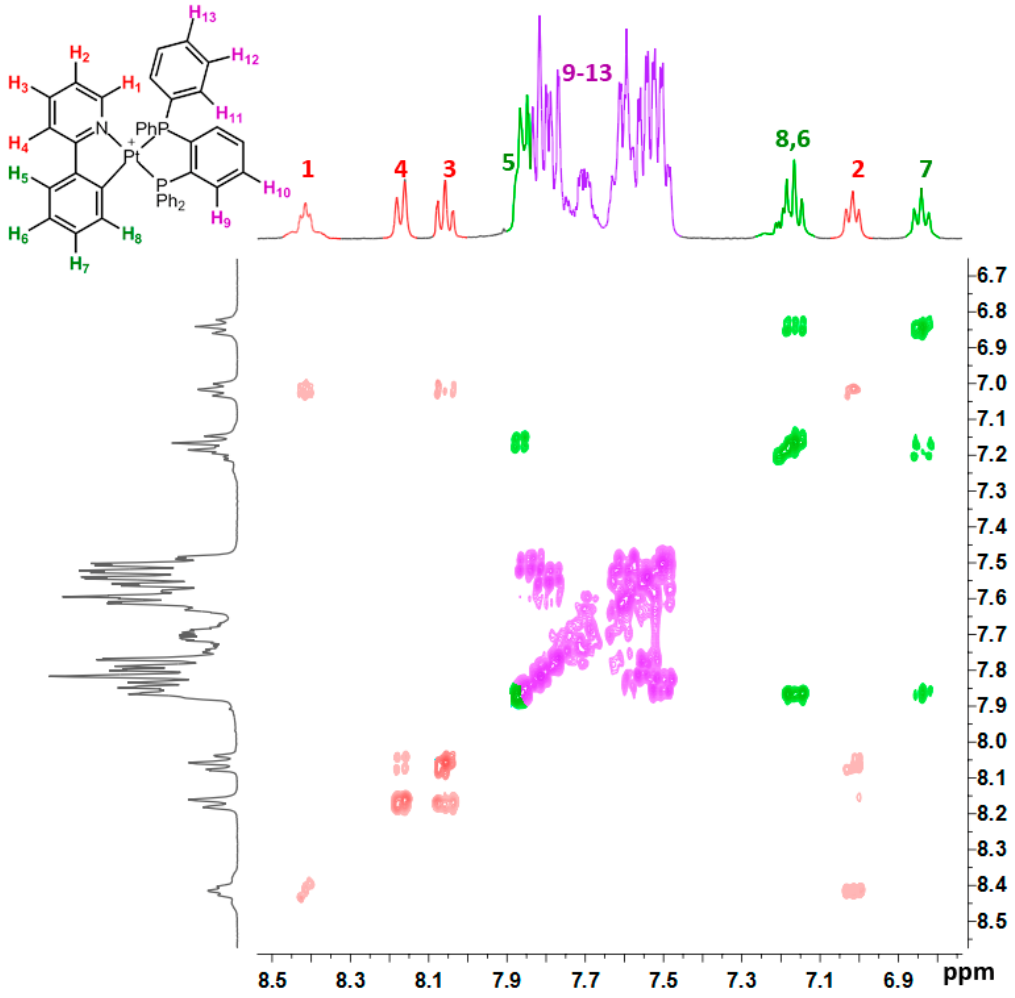

Figure S11. ^{1}H-^{1}H COSY NMR spectrum of **Pt1**, CD_3OD, 298K.

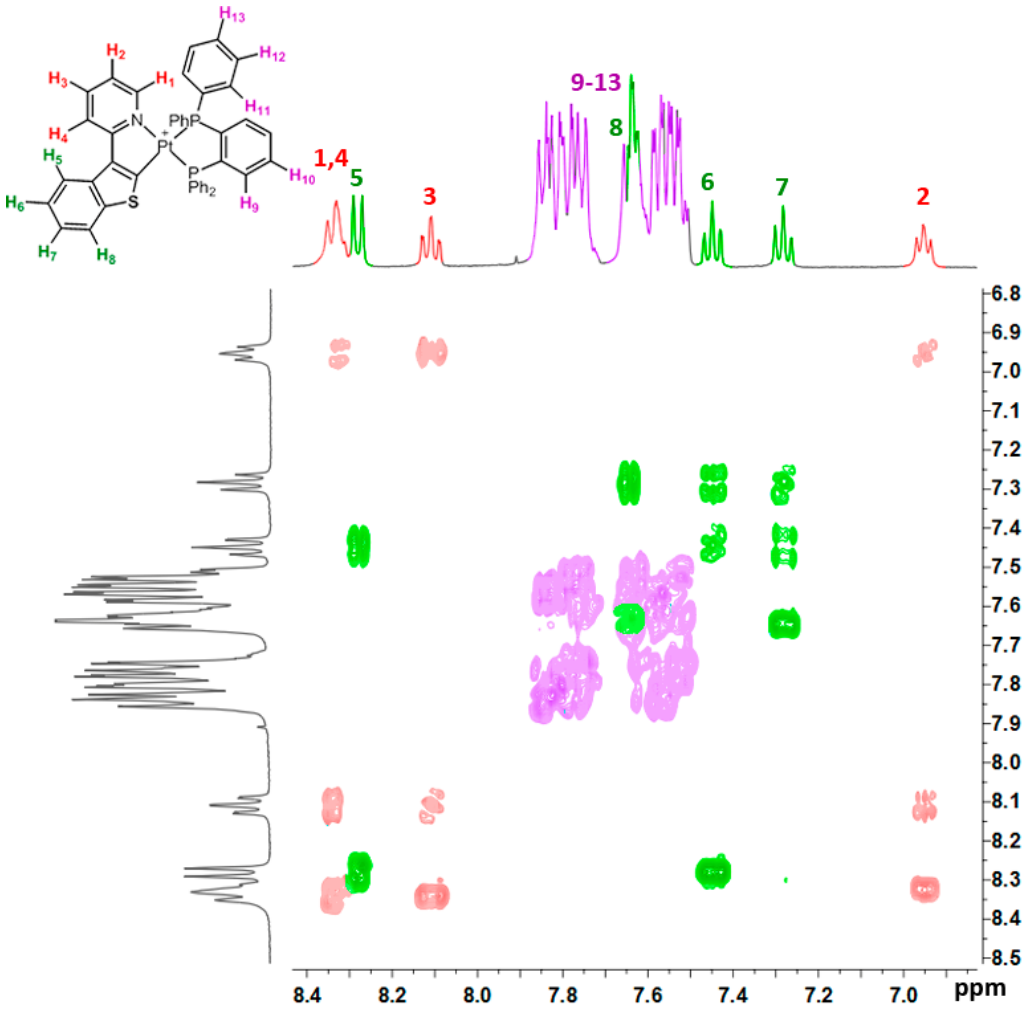

Figure S12. ^{1}H-^{1}H COSY NMR spectrum of **Pt2**, CD_3OD, 298K.

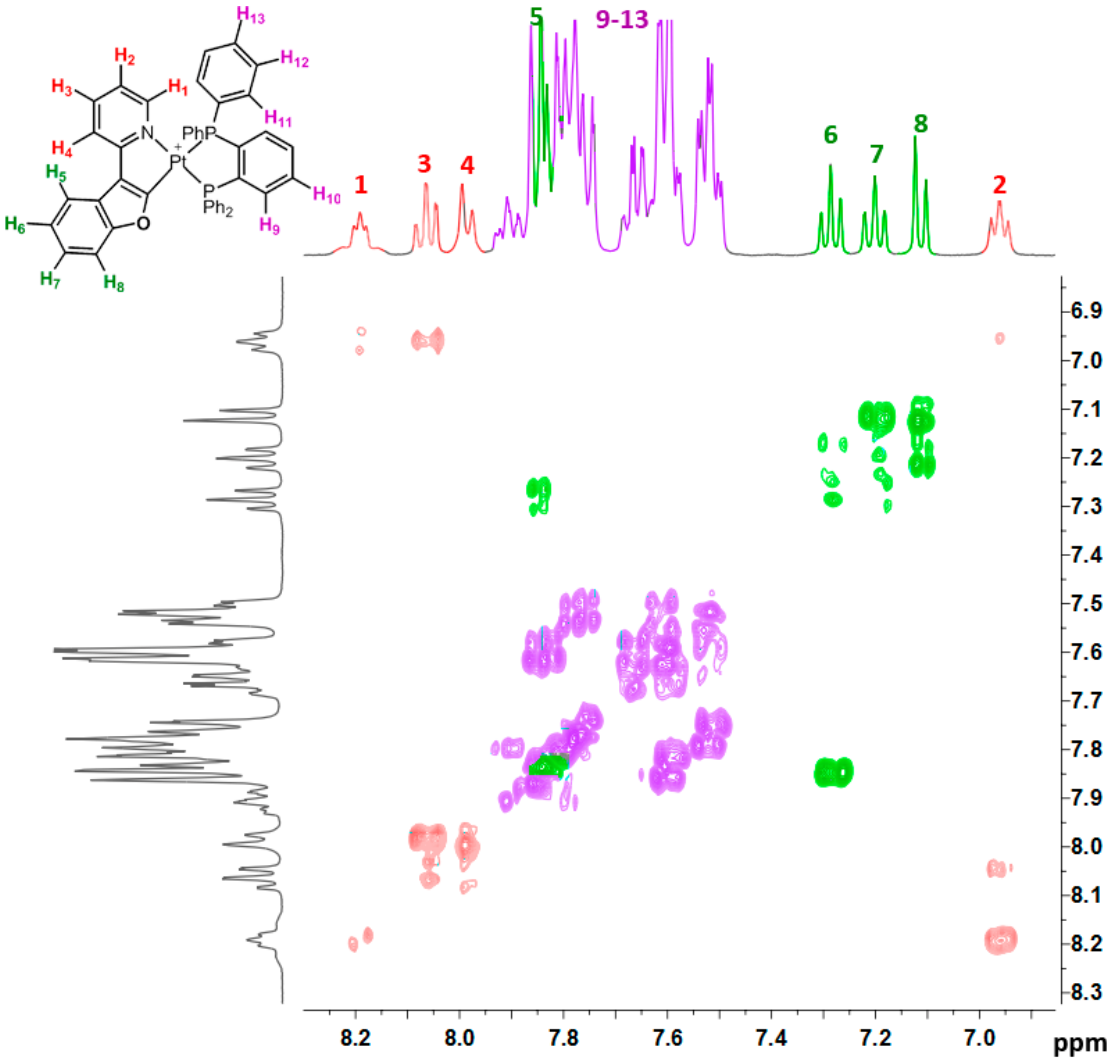

Figure S13. ^{1}H-^{1}H COSY NMR spectrum of **Pt3**, CD_3OD, 298K.

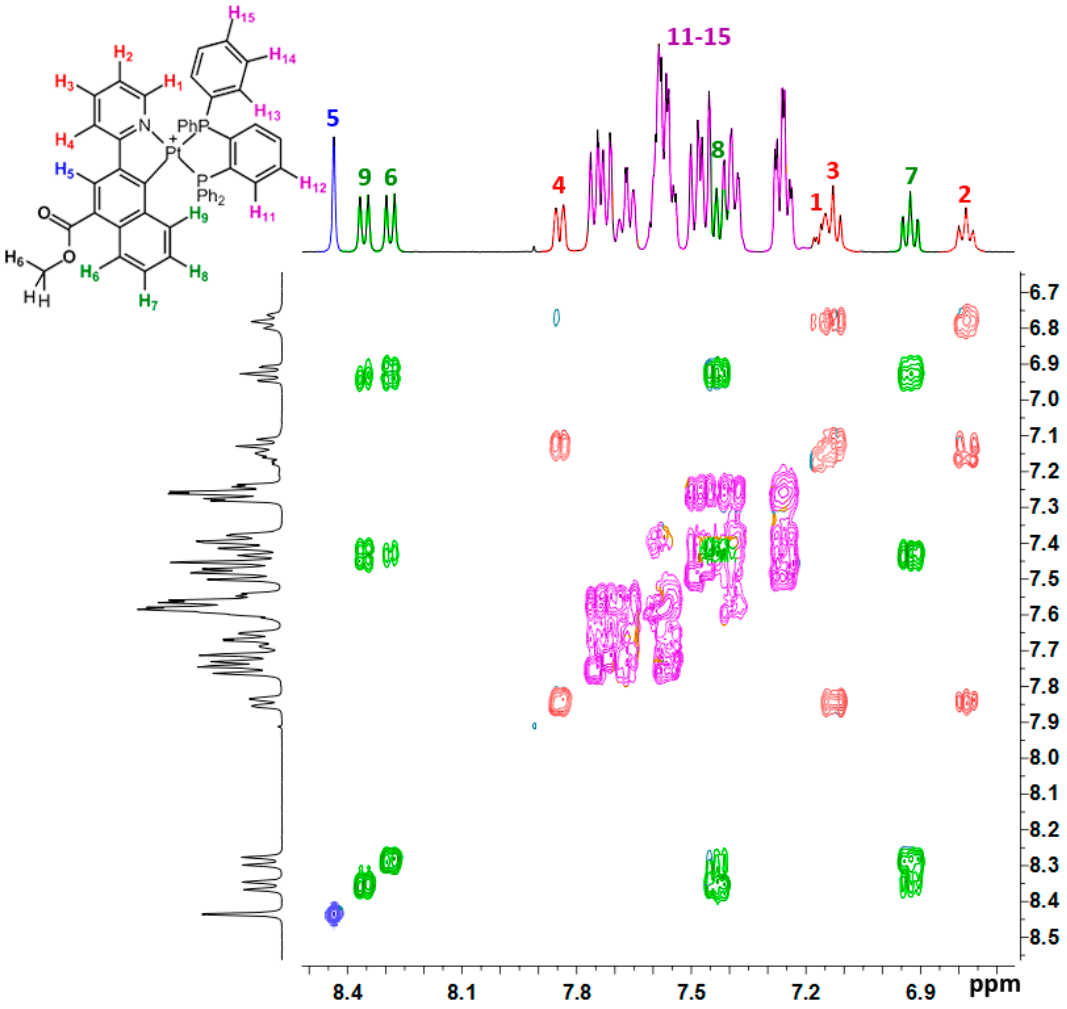

Figure S14. ^{1}H-^{1}H COSY NMR spectrum of **Pt4**, CD_3OD, 298K.

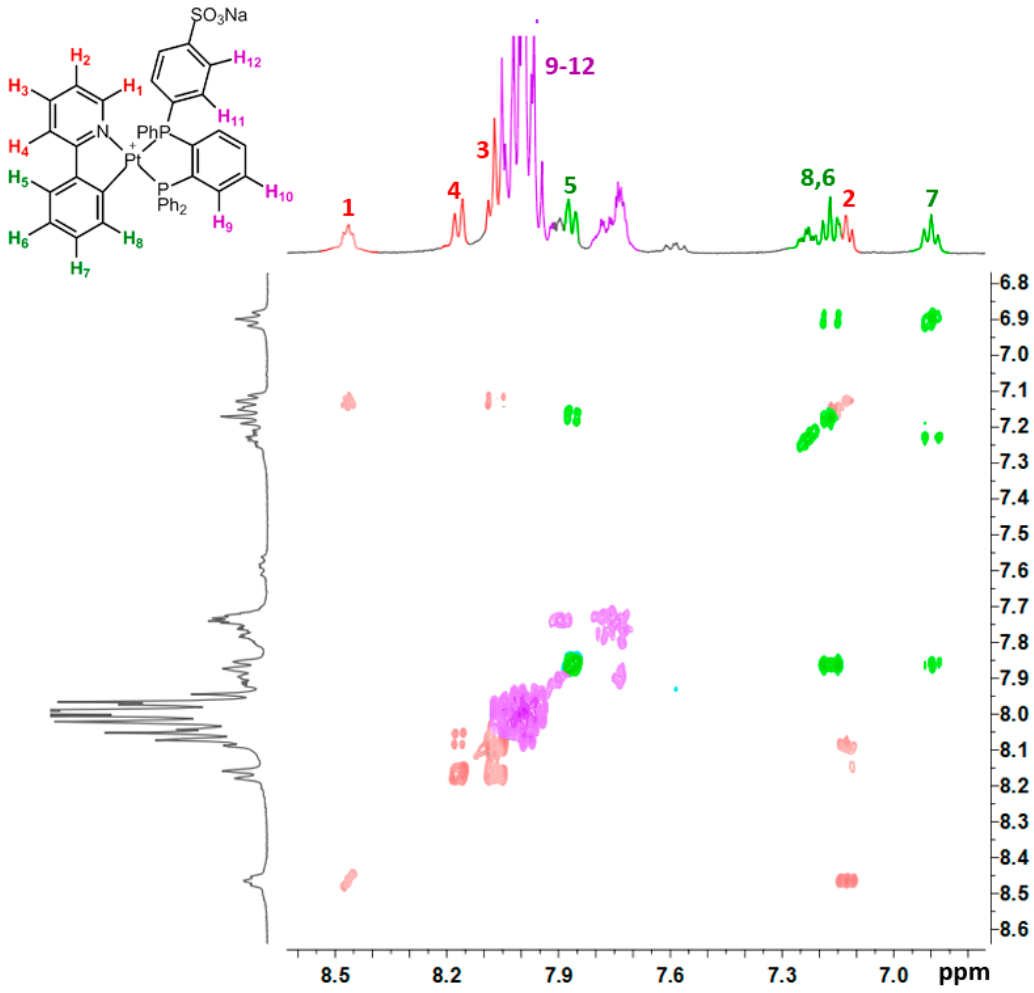

Figure S15. ^{1}H-^{1}H COSY NMR spectrum of **Pt1***, CD_3OD, 298K.

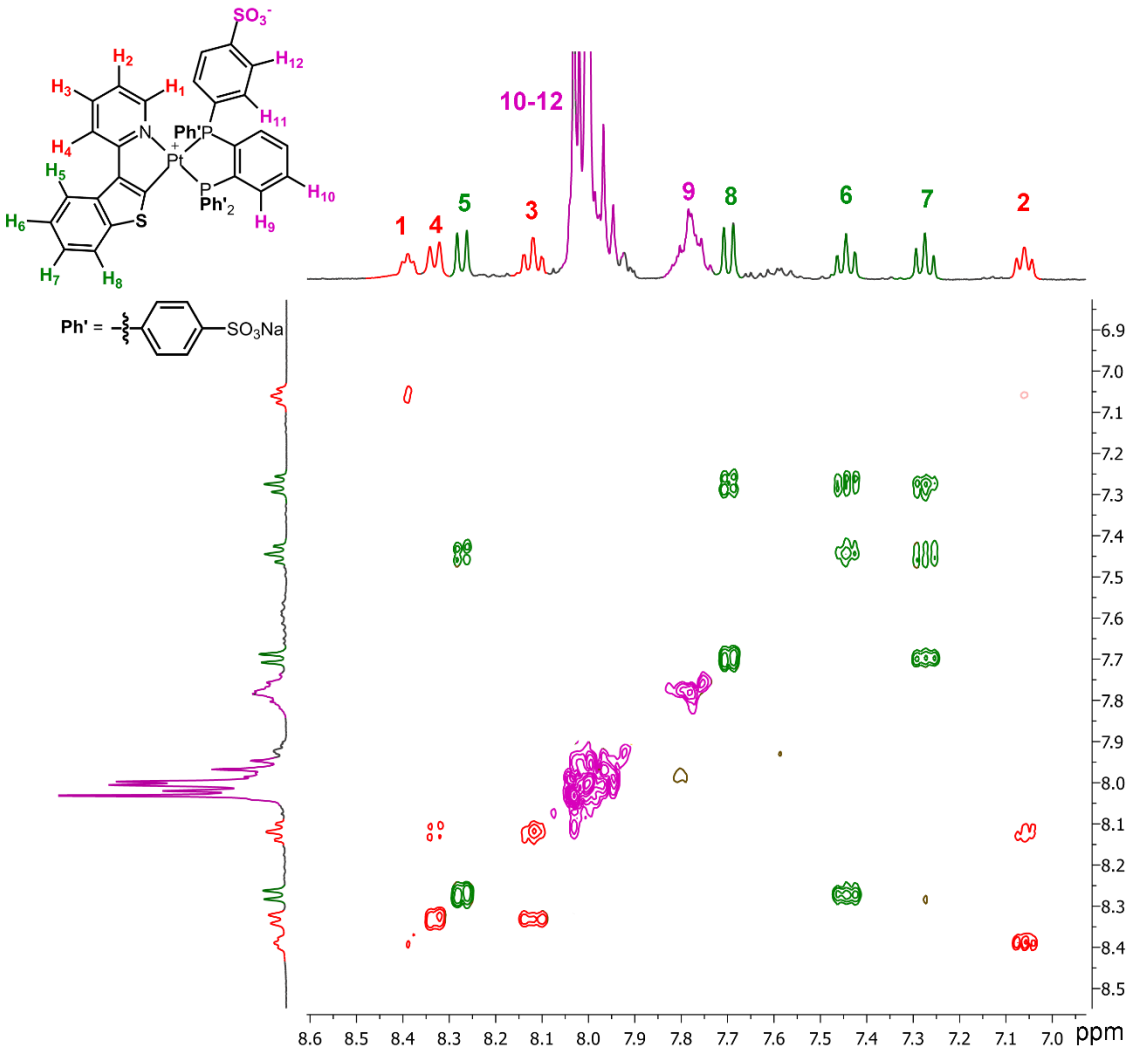

Figure S16. ^{1}H-^{1}H COSY NMR spectrum of **Pt2***, CD_3OD, 298K.

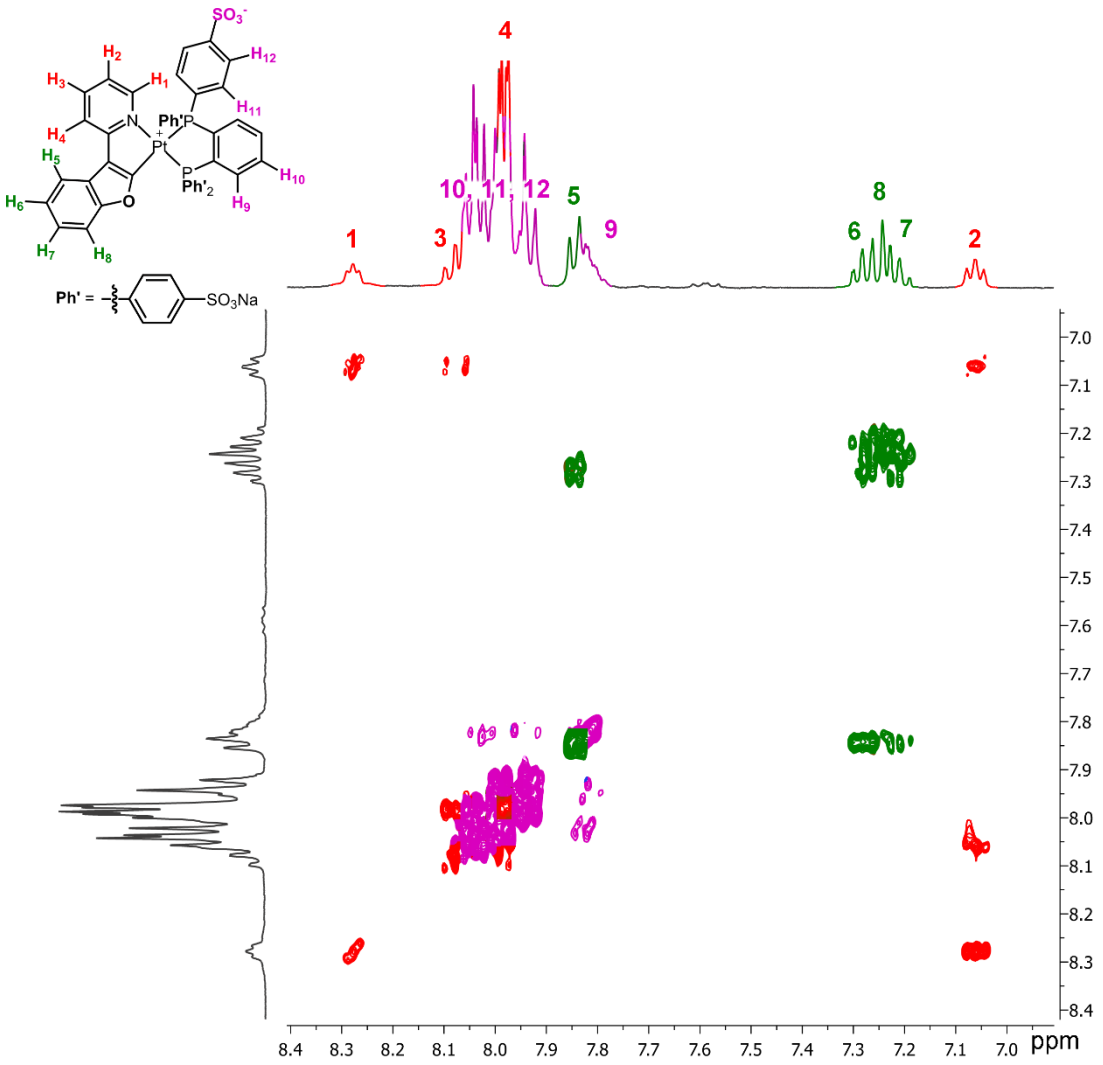

Figure S17. ^{1}H-^{1}H COSY NMR spectrum of **Pt3***, CD_3OD, 298K.

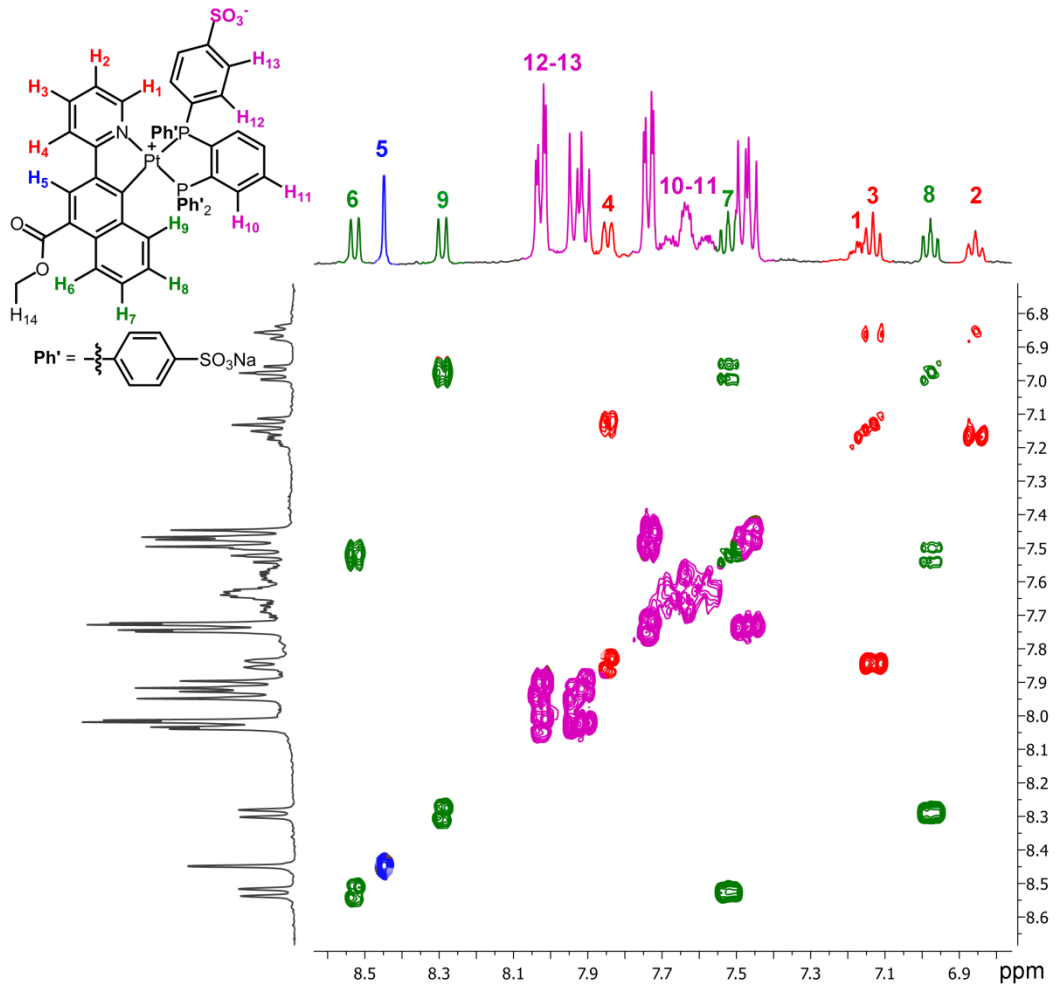

Figure S18. ^{1}H-^{1}H COSY NMR spectrum of **Pt4***, CD_3OD, 298K.

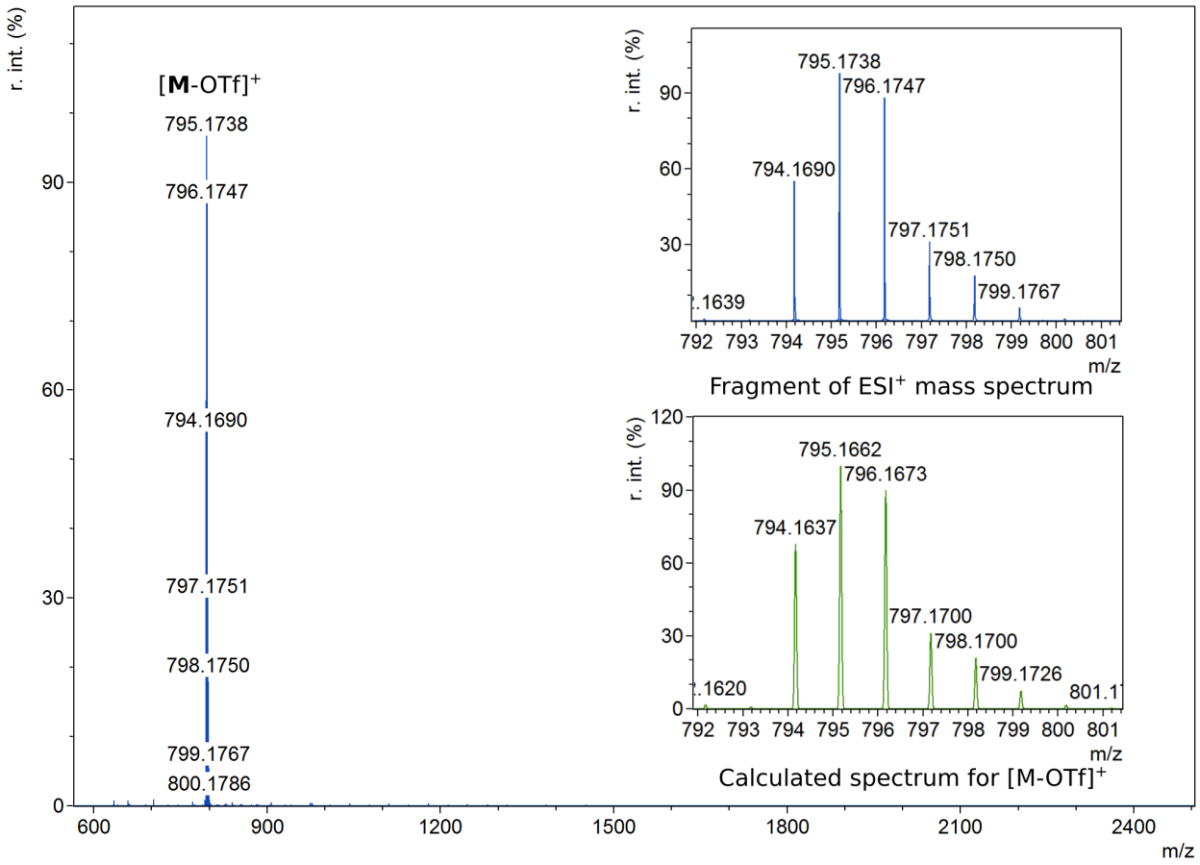

Figure S19. ESI$^+$ mass spectrum of complex **Pt1**.

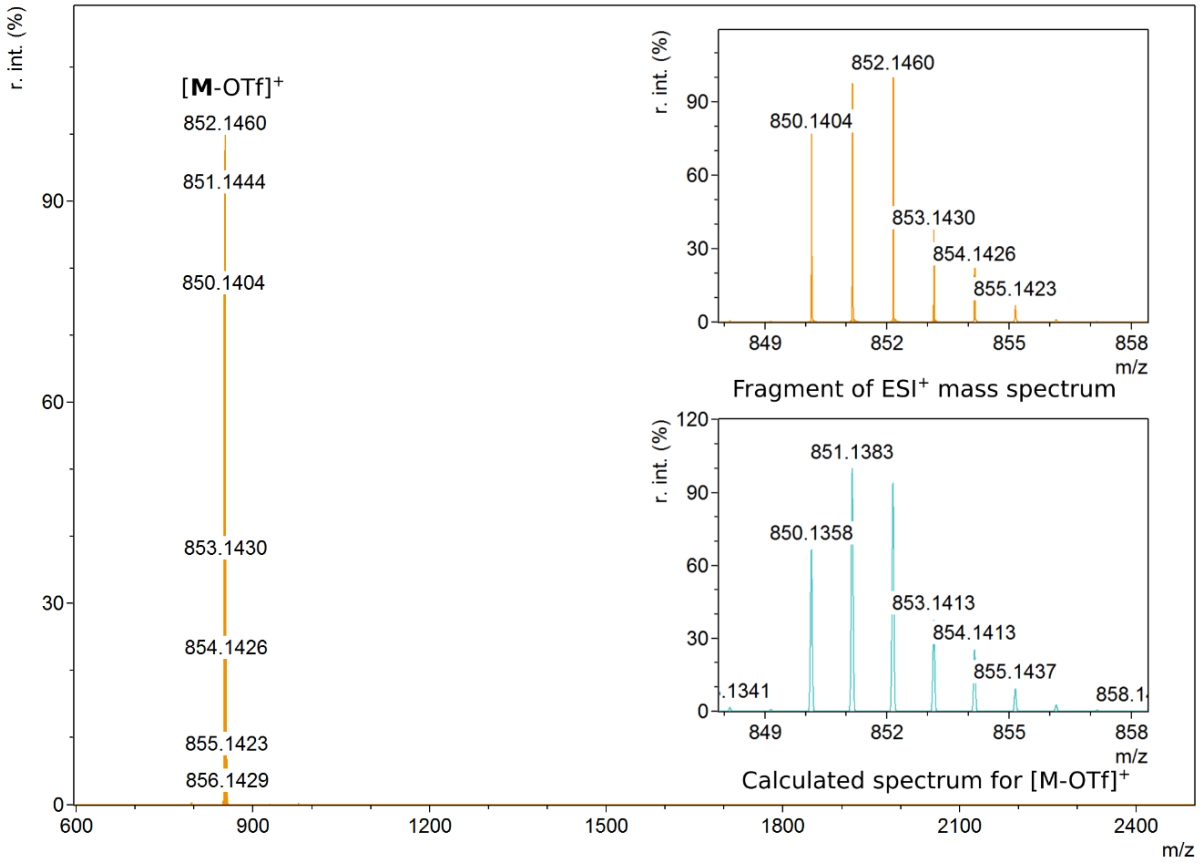

Figure S20. ESI$^+$ mass spectrum of complex **Pt2**.

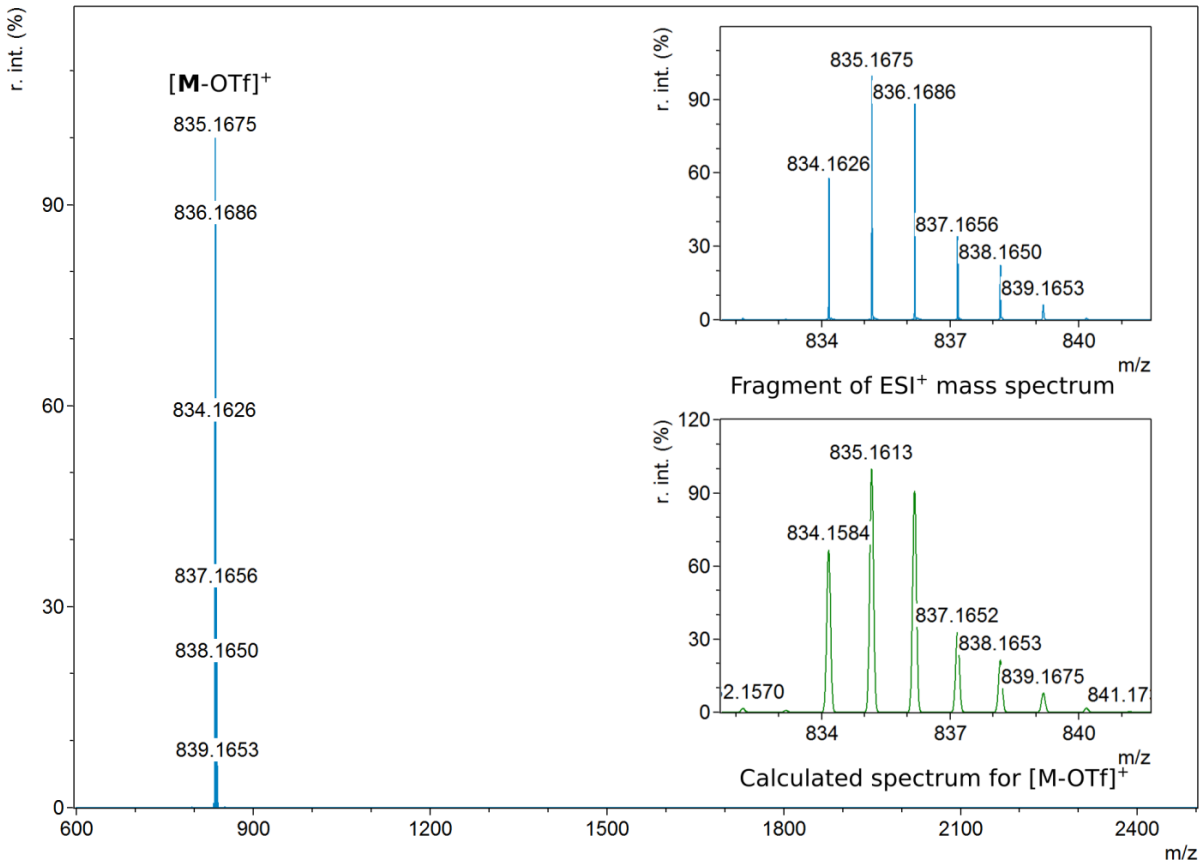

Figure S21. ESI$^+$ mass spectrum of complex **Pt3**.

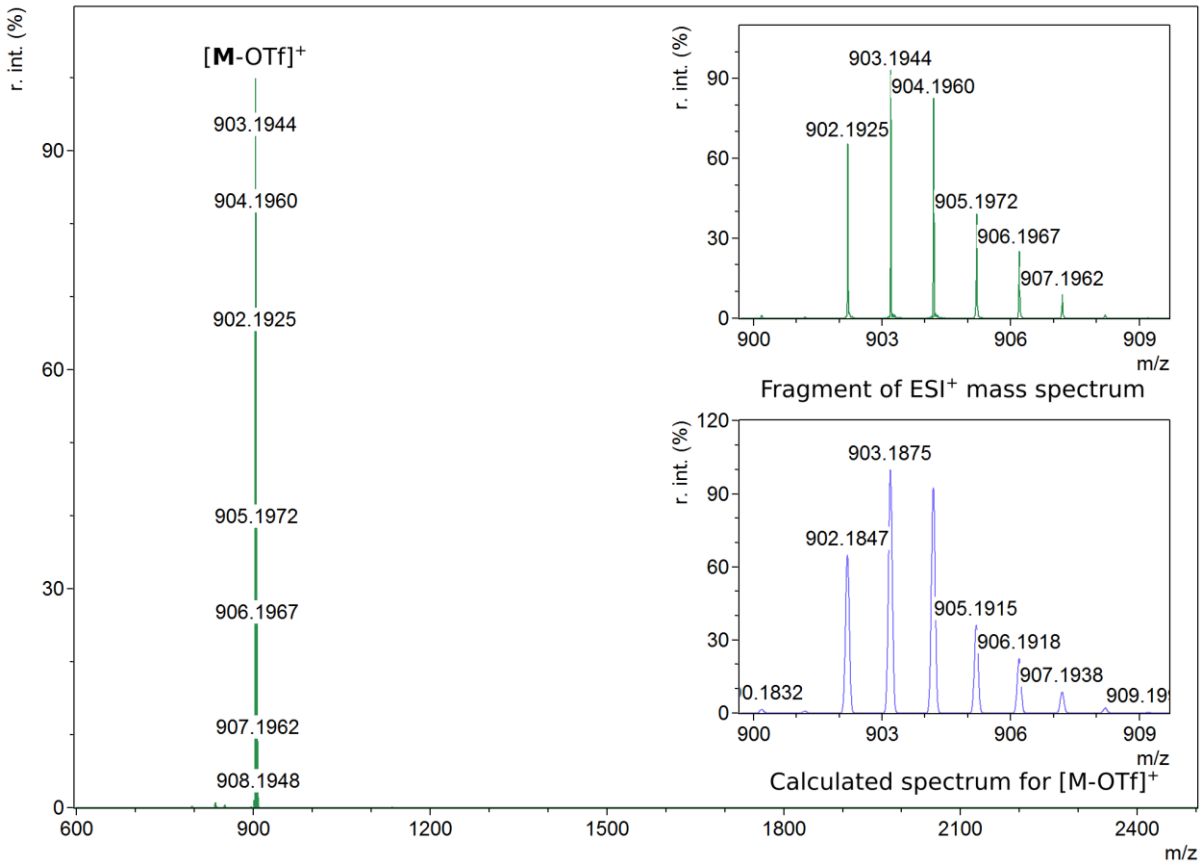

Figure S22. ESI$^+$ mass spectrum of complex **Pt4**.

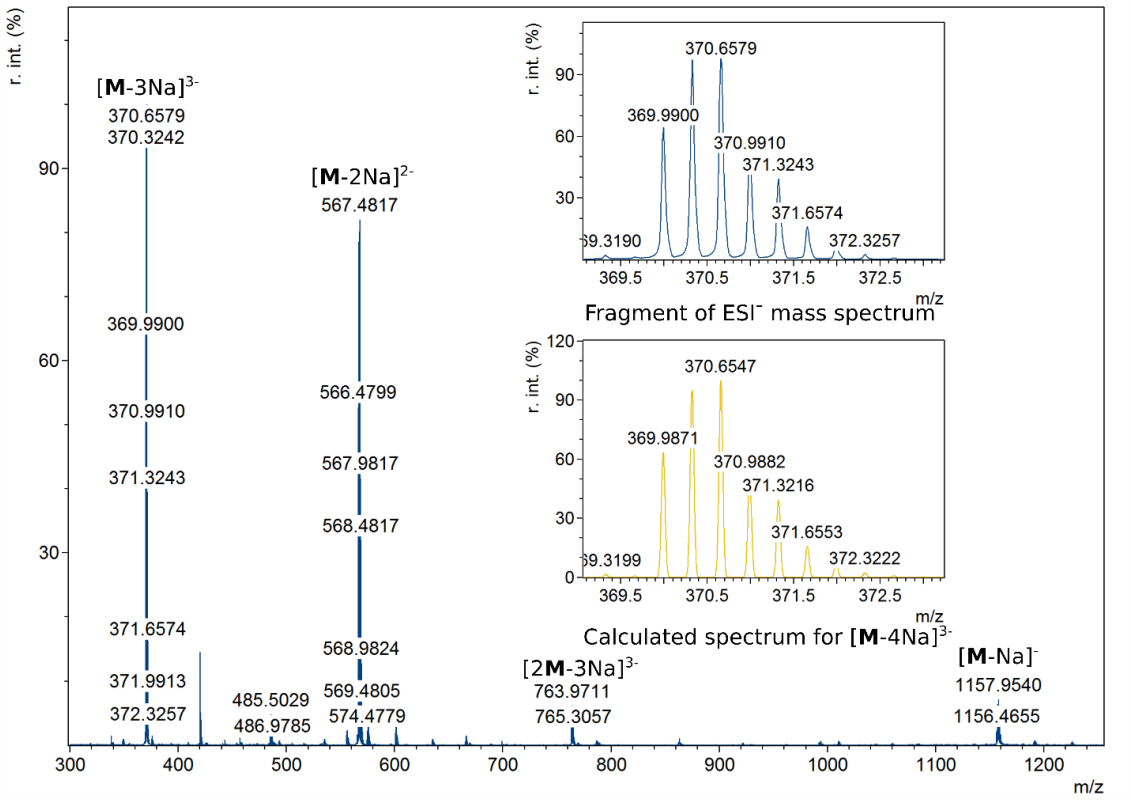

Figure S23. ESI$^-$ mass spectrum of complex **Pt1***.

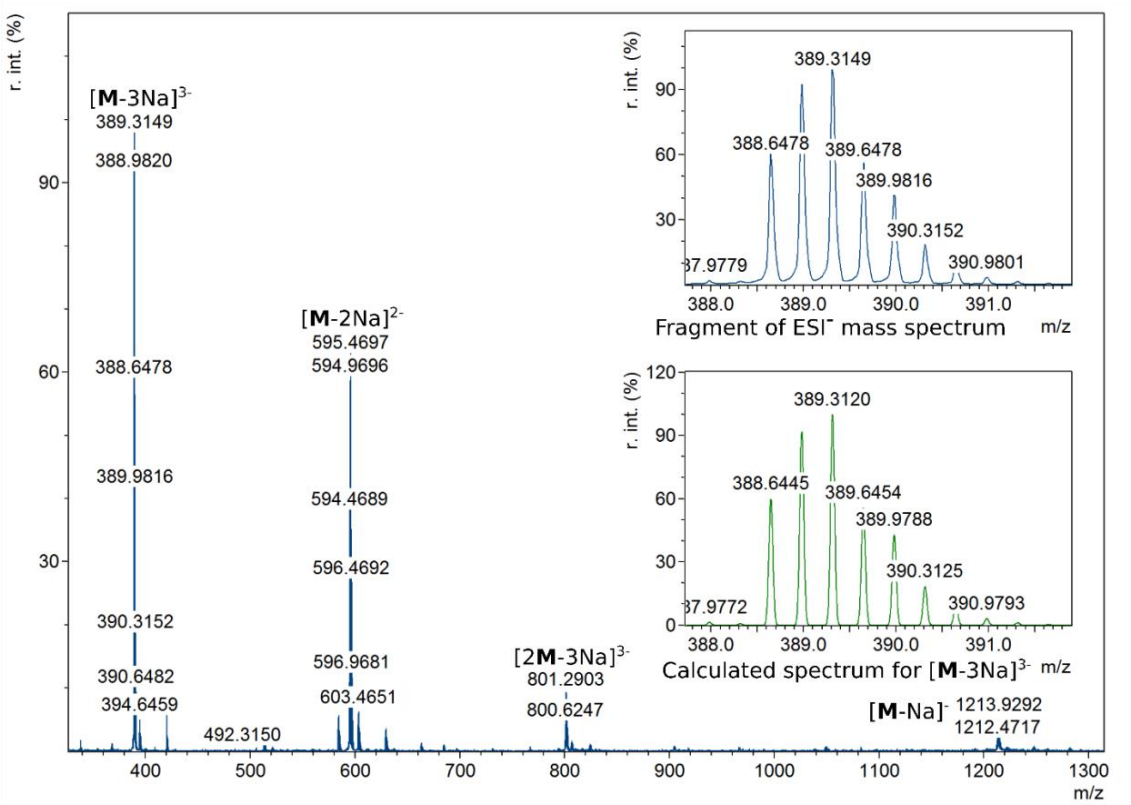

Figure S24. ESI$^-$ mass spectrum of complex **Pt2***.

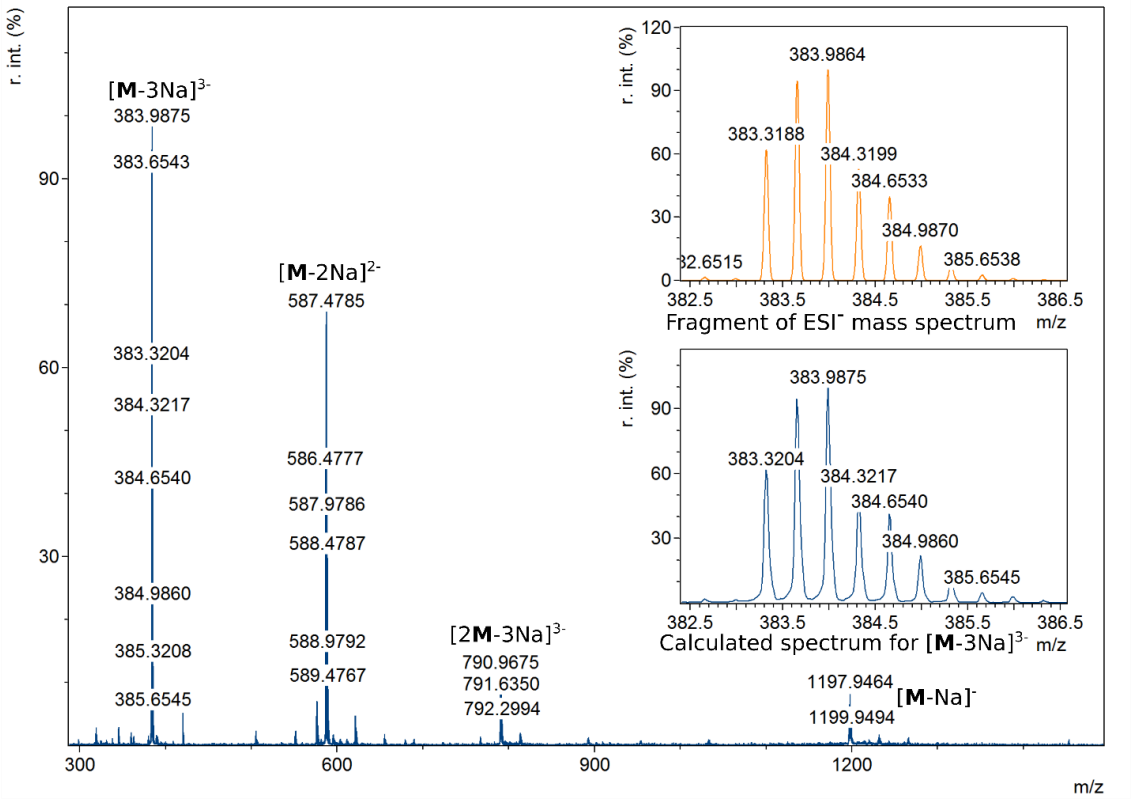

Figure S25. ESI$^-$ mass spectrum of complex **Pt3***.

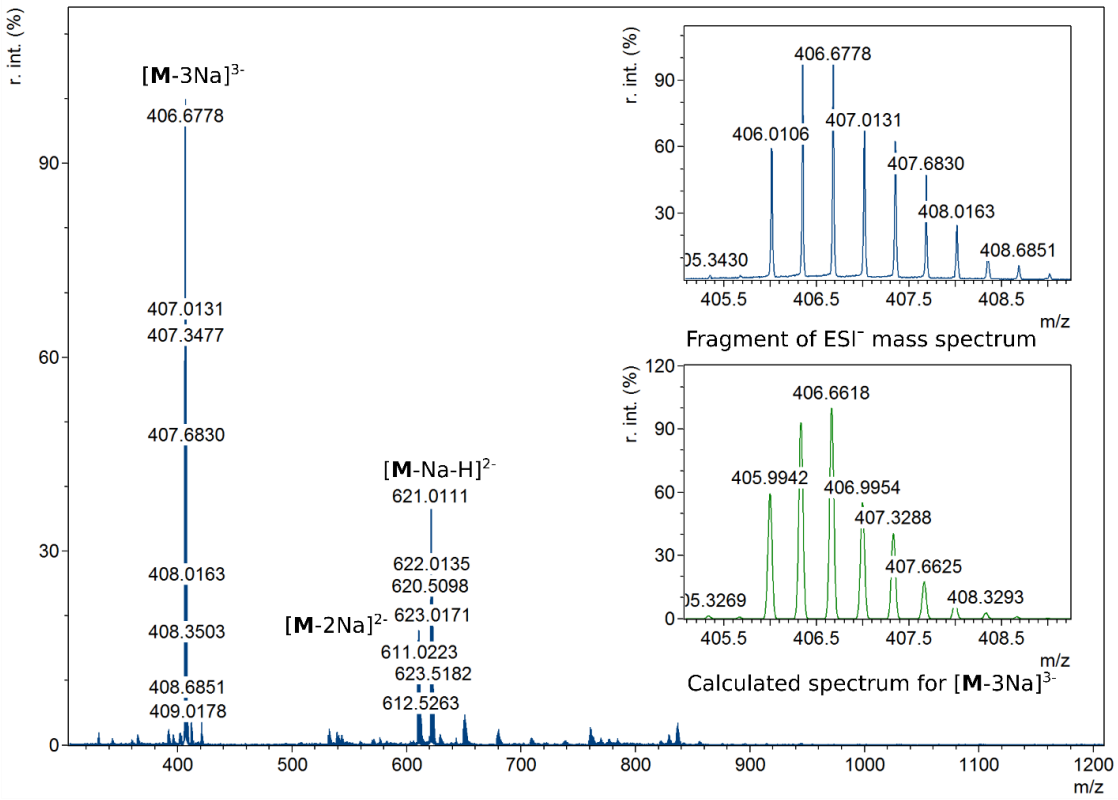

Figure S26. ESI$^-$ mass spectrum of complex **Pt4***.

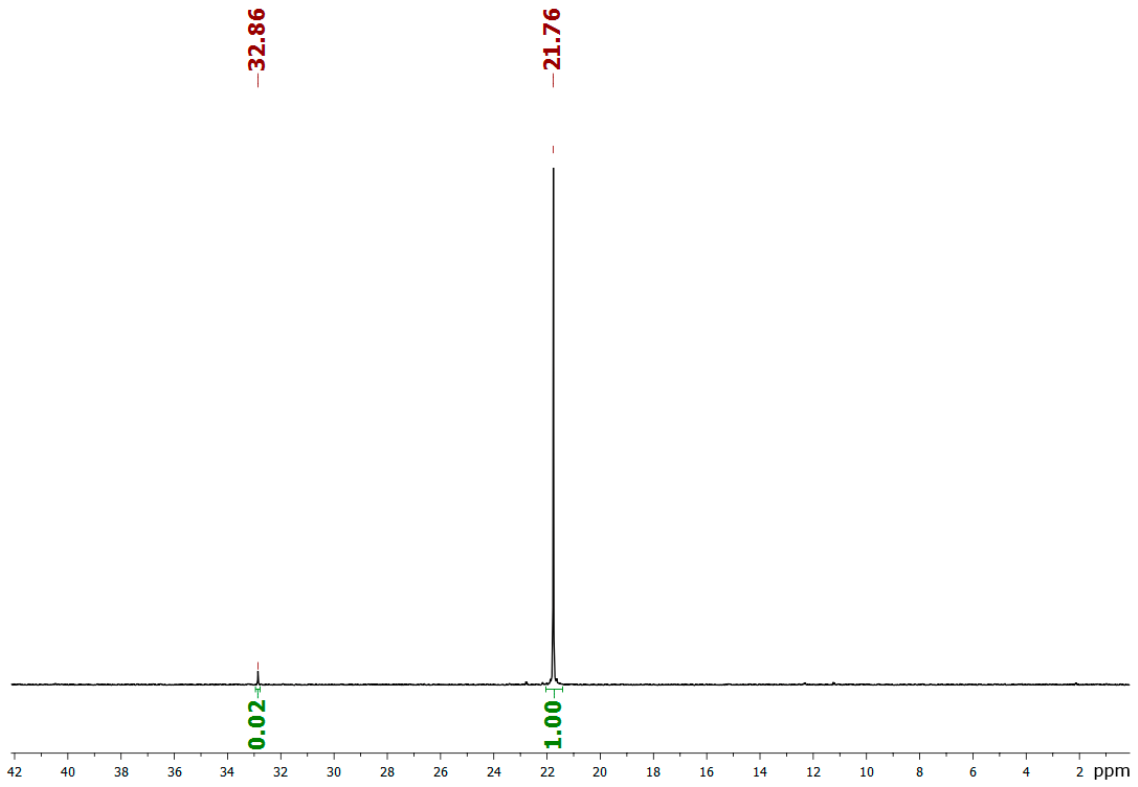

Figure S27. ^{31}P NMR spectrum of **Ir1***, CD_3OD, 298K.

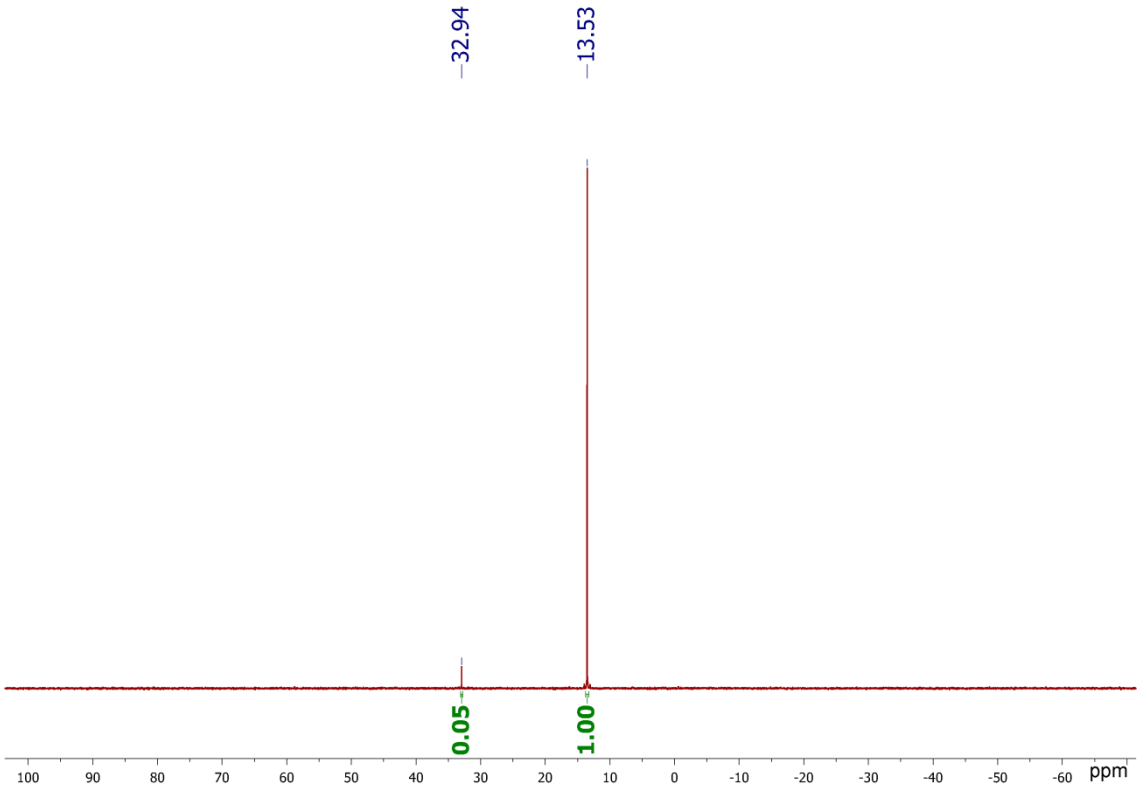

Figure S28. ^{31}P NMR spectrum of **Ir2***, CD_3OD, 298K.

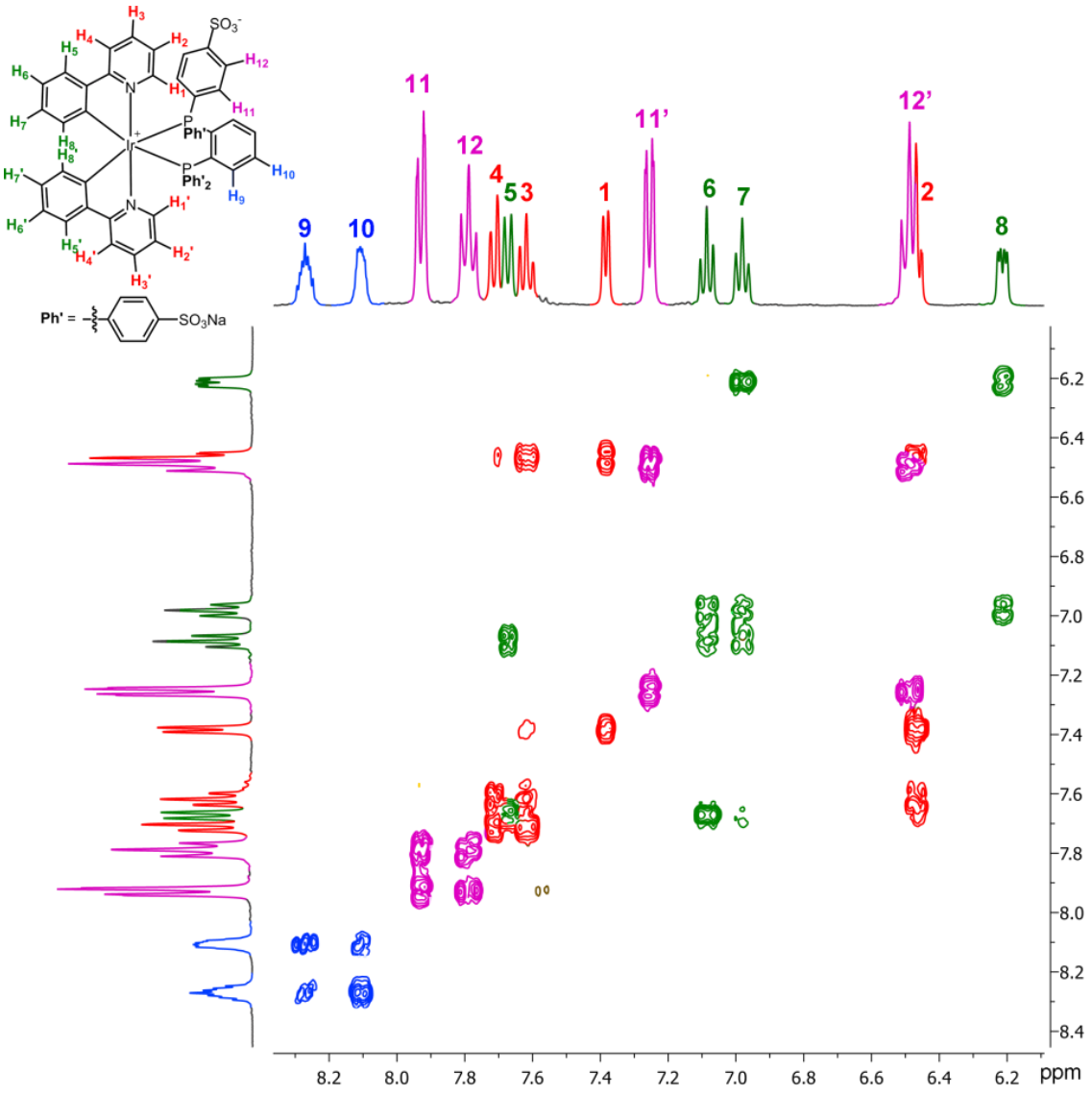

Figure S29. ^{1}H-^{1}H COSY NMR spectrum of **Ir1***, CD_3OD, 298K.

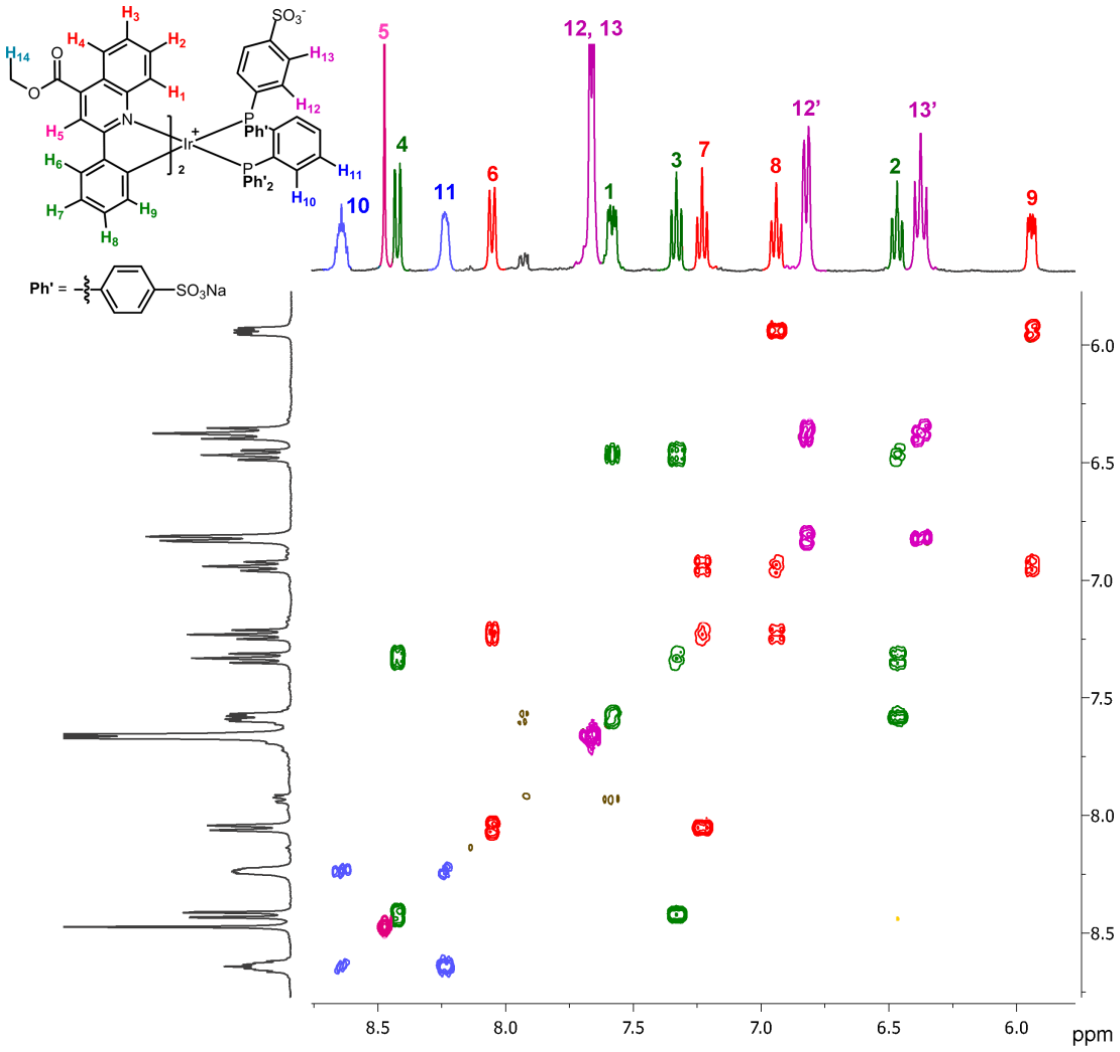

Figure S30. ^{1}H-^{1}H COSY NMR spectrum of **Ir2***, CD_3OD, 298K.

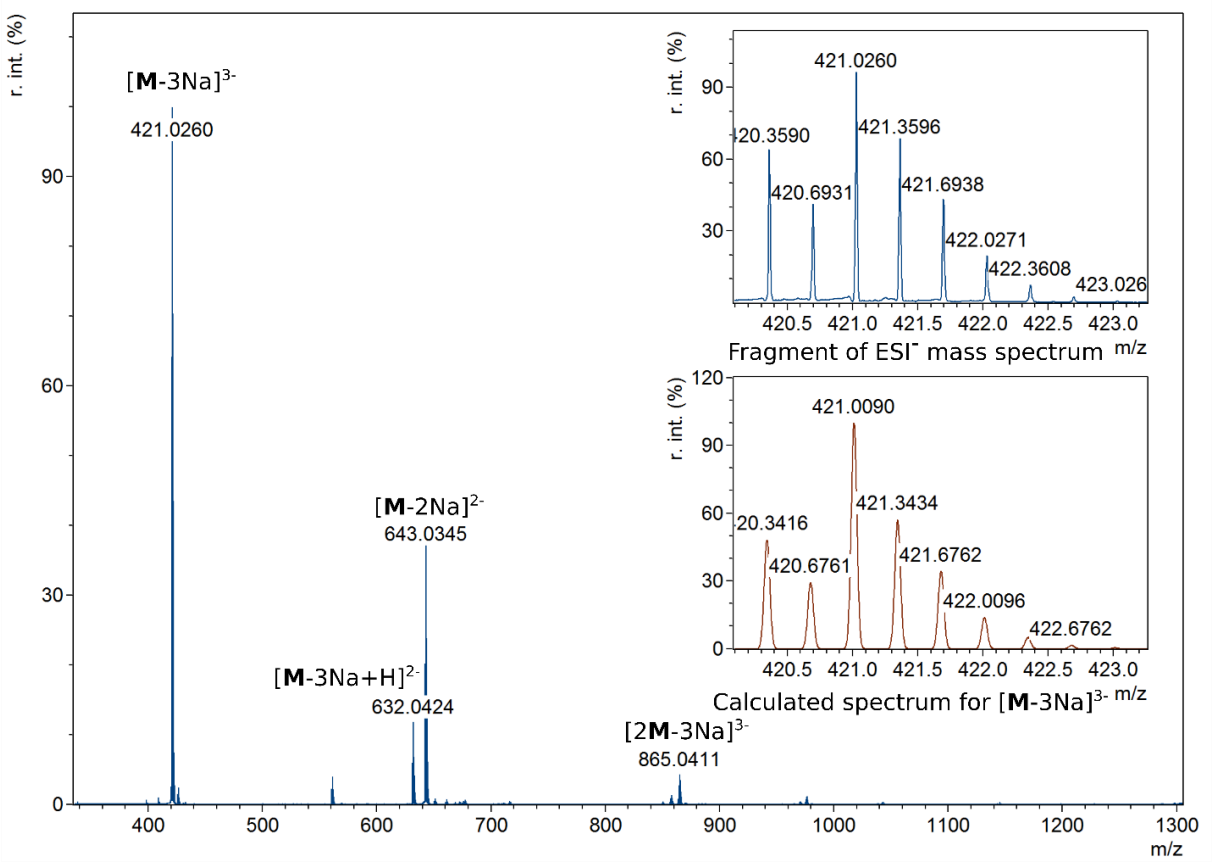

Figure S31. ESI$^-$ mass spectrum of complex **Ir1***.

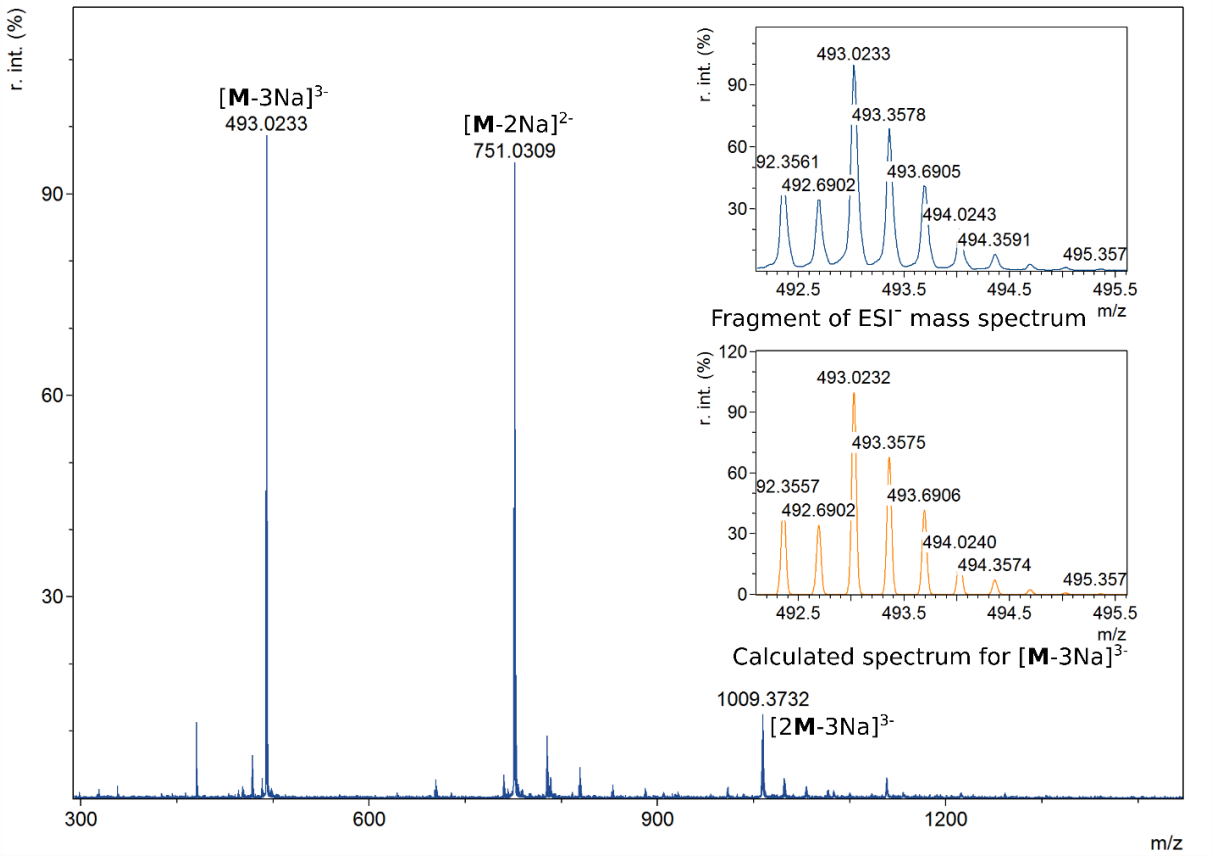

Figure S32. ESI$^-$ mass spectrum of complex **Ir2***.

Section 2. Photophysical and spectroscopic properties of platinum and iridium complexes in solid state and solution

Emission measurements in solid state were carried out with a Fluorolog 3 spectrofluorimeter (JY Horiba Inc.). Direct quantum yield measurements of the crystalline samples were performed at room temperature with an integrating sphere from Quanta-phi. Lifetimes in solid state were determined by the Time-Correlated Single Photon Counting (TCSPC) method. The lifetime data were fit using the Jobin-Yvon software package and the Origin 9.0 program.

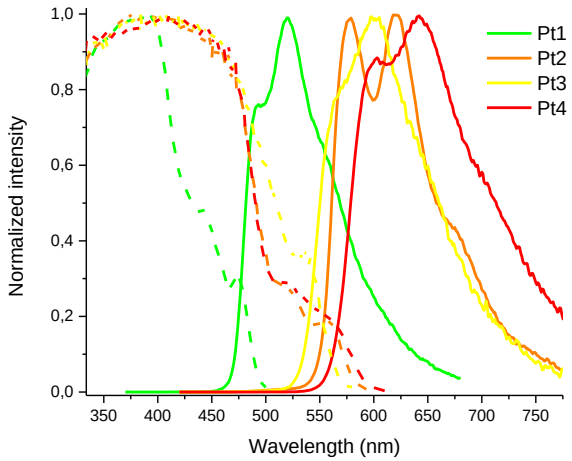

Figure S33. Emission spectra (solid line) of platinum complexes in solid state (λ_{ex} = 365 nm) and excitation spectra (dashed line) (λ_{em} (**Pt1**) = 520 nm, λ_{em} (**Pt2**) = 620 nm, λ_{em} (**Pt3**) = 600 nm, λ_{em} (**Pt4**) = 640 nm).

Table S3. Photophysical properties of platinum compounds in solid state.

№	λ_{ex}, nm	λ_{em}, nm	τ_{obs}[a], μs	Φ, %
Pt1	424sh, 442, 475	493, 520, 550	23.15	25.31
Pt2	517sh, 557	578, 620, 670sh, 730sh	19.65	7.73
Pt3	440, 537	570sh, 600, 640sh, 700sh	19.40	16.45
Pt4	450, 523, 558	603, 642, 700sh	19.00	4.46

[a] average emission lifetimes for the two-exponential decay determined using the equation $\tau_{obs} = (A_1\tau_1^2 + A_2\tau_2^2)/(A_1\tau_1 + A_2\tau_2)$, where A_i is the weight of the i-exponent.

The absorption spectra of platinum complexes both in dichloroethane (**Pt1**-**Pt4**, Fig. S33) and in aqueous solutions (**Pt1***-**Pt4***, Fig. S34) display intense high energy bands (λ_{abs} < 300 nm), which can be assigned to IL transitions localized at aromatic systems of metalating and diphosphine ligands [3]. The red shifted bands of lower intensity extended to ca. 370 nm (**Pt1** and **Pt1***) and

425 nm (**Pt2**-**Pt4** and **Pt2***-**Pt4***) evidently originate from MLCT transitions associated mainly with metalating ligands with a possible contribution of LLCT processes [3,4]. This conclusion is also supported by a stronger red shift of lowest energy absorption for the complexes containing developed aromatic system compared to that of the congeners with the simpler phenylpyridine ligand.

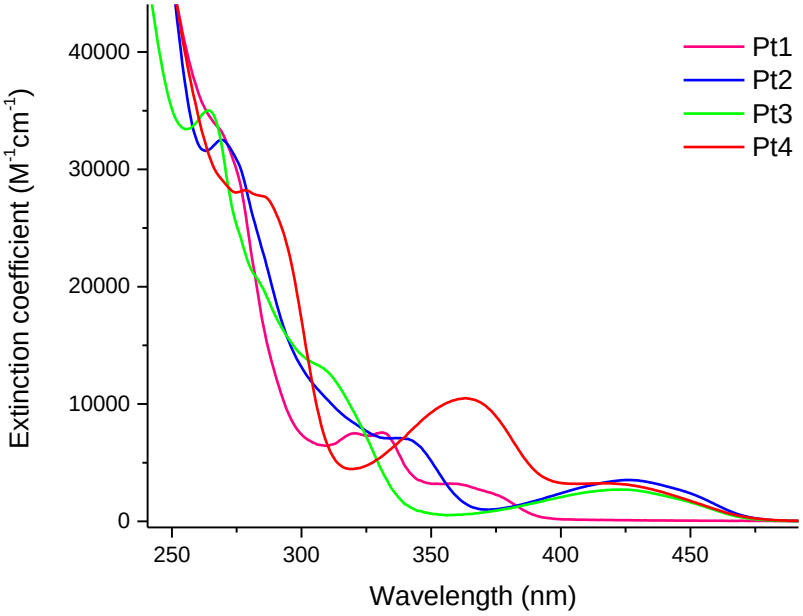

Figure S34. Absorption spectra of complexes **Pt1**-**Pt4** in DCE.

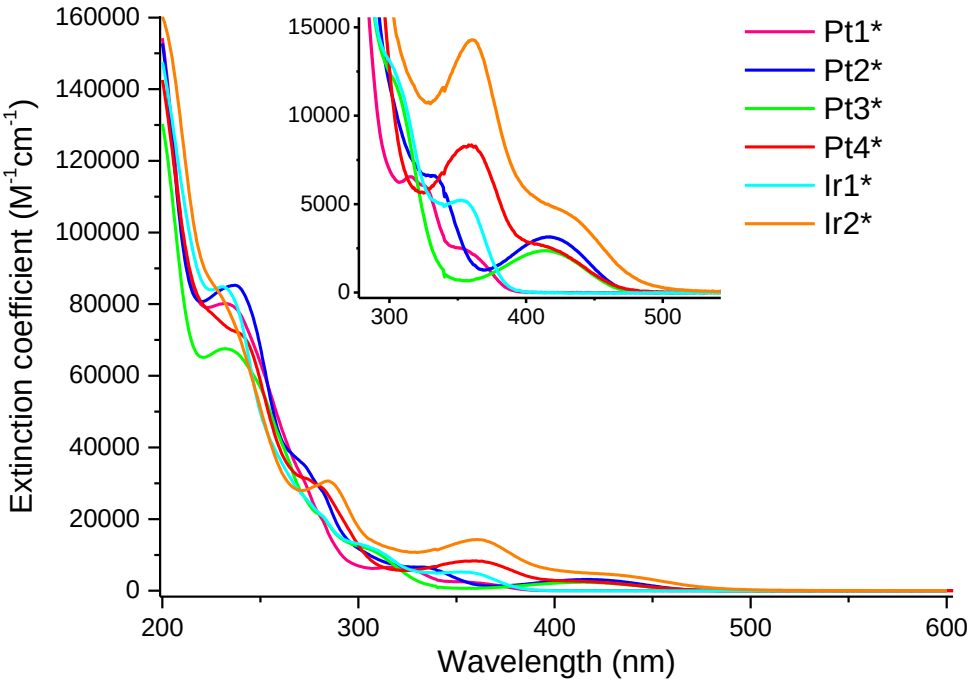

Figure S35. Absorption spectra of the **Pt1*- Pt4*** and **Ir1*, Ir2*** complexes in aqueous solution.

A weak or even negligible emission of this type of complexes in solution is not exceptional [3,4,9–11] because of nonradiative deactivation of excited molecules by facile interaction with the solvent in fluid state at room temperature. It is interesting that emission quenching of water-soluble complexes containing sulfonated diphosphine in aqueous solution is somewhat lower compared to non-sulfonated analogues (see QY and lifetime parameters of the pairs **PtX*-PtX**, see Table 1, main text) that may be due to shielding effect of the $-SO_3^-$ substituents in the former type of compounds.

Emission profiles as well as emission maxima of sulfonated and non-sulfonated platinum complexes are essentially similar, pointing to emission from the excited state of the same nature, characteristics of which are independent of the donor properties of the diphosphines. The effect of metalating ligands is more pronounced and also appears as much larger Stokes shift in the **Pt4** and **Pt4*** complexes, which exceeds 200 nm, cf. the value of ca. 100 nm for the other platinum emitters, see Figure 1. This effect may be related to the presence of electron accepting substituent in the pyridyl fragment of the aromatic system as well as to additional vibrational/rotational relaxation of the singlet MLCT excited state upon intersystem crossing into the corresponding triplet for the compounds containing carboxyl-ester substituent in the C^N ligand. This observation indicates

once more a major role of the C^N ligand orbitals in the emissive excited states of the metalated platinum complexes.

In agreement with the data obtained in previously published research [7], the high energy absorption of **Ir1*** (230-350 nm) should be assigned to IL(π–π*) transitions whereas weaker long wavelength bands are determined by spin-allowed ^{1}MLCT and spin-forbidden ^{3}MLCT transitions, see Fig. 1, main text. Accordingly, the ^{3}IL transition was suggested to dominate in vibronically structured emission band at ca. 490 nm [7]. However, the presence of rather strong long wavelength band in the excitation spectrum of **Ir1*** with the maximum at 355 nm stretching down to 400 nm implies considerable admixture of the MLCT states in the emission observed. The latter component of excitation is evidently even stronger in the case of **Ir2*** where the low energy absorption and excitation extend down to 500 nm and structureless emission band is red-shifted to 620 nm. It has to be mentioned that the lifetime and QY data for **Ir1** given in early publications are strongly inconsistent even taking into account different solvents and aeration conditions. For example, the values of QY = 0.0068 and lifetime 502 ns were given for **Ir1** in aerated MeCN solution[6], whereas analogous measurements in degassed CH_2Cl_2 [7] gave QY = 0.16 and dual lifetime 80 and 2 ns. The latter result implies extremely fast deactivation of the triplet excited state that is hardly compatible with rather high quantum yield. In our experiments, we obtained self-consistent data with the QY values of a few percent and lifetime in microsecond domain, the lower QY corresponding to the lower lifetime.

Two photon absorption (TPA) cross section.

The open aperture Z-scan experiments were conducted to measure the two photon absorption properties of the metal complexes. In the case of our experiment, a mode-locked Ti:sapphire laser (Tsunami, Spectra Physics) produced a single Gaussian pulse, then coupled to a regenerative amplifier that finally generated a ~ 180 fs, 1 mJ pulse (800 nm, 1 kHz). The pulse energy, after proper attenuation, was adjusted to 1.80-2.10 μJ appropriate to TPA experiment. At the step of measurement, the laser beam was focused and passed through a 1.00 mm quartz cell with the beam radius of ~ 3.82×10^{-3} cm at the focal position. As the quartz cell was moved stepwise along the laser beam direction (z-axis), the intensity of transmitted laser was detected by the photodiode. Each dataset was obtained by an average of four measurements The TPA-resulting decrease in transmittance, T(z), can be fitted with Eq. S1 including the TPA coefficient (β):

$$\mathrm{T(z)} = \sum_{n=0}^{\infty} \frac{(-q)^n}{(n+1)^{3/2}}; q = \frac{\beta I_0 L}{1+\frac{z^2}{z_0^2}} \quad (S1)$$

where n is an integer number from 0 to ∞ and has been properly truncated at n = 1000 for calculation. I_0 is the input intensity, and L is the sample length, while z represents the sample position with respect to the focal plane. z_0 represents the diffraction length of the incident beam (Rayleigh range). Once obtaining the TPA coefficient (β), TPA cross section (σ_2) can be extracted according to Eq. S2:

$$\beta = \frac{\sigma_2 N_A d \times 10^{-3}}{h\nu} \quad (S2)$$

where N_A is the Avogadro constant, hν is the incident photon energy, and d is the sample concentration.

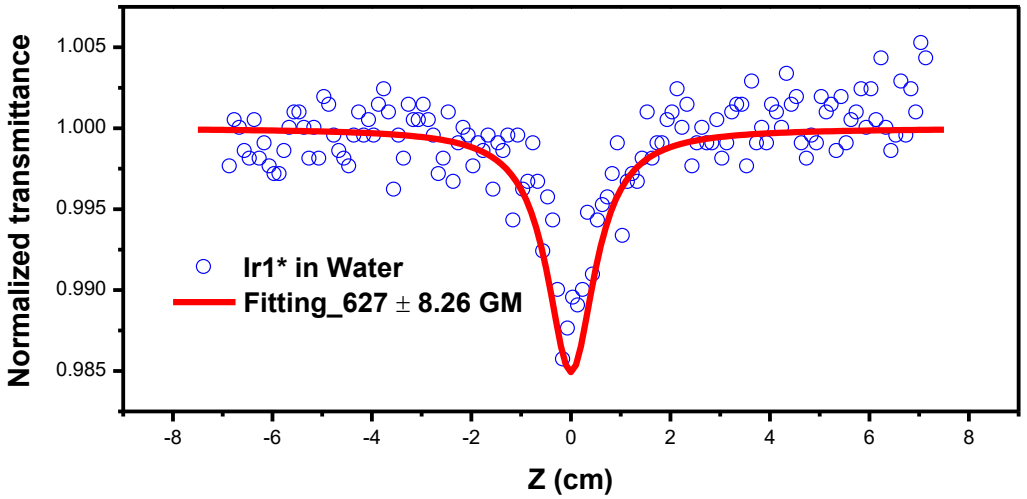
Normalized transmittance
1.005
1.000
0.995
0.990
0.985
Ir1* in Water
Fitting_627 ± 8.26 GM
-8
-6
-4
-2
0
2
4
6
8
Z (cm)

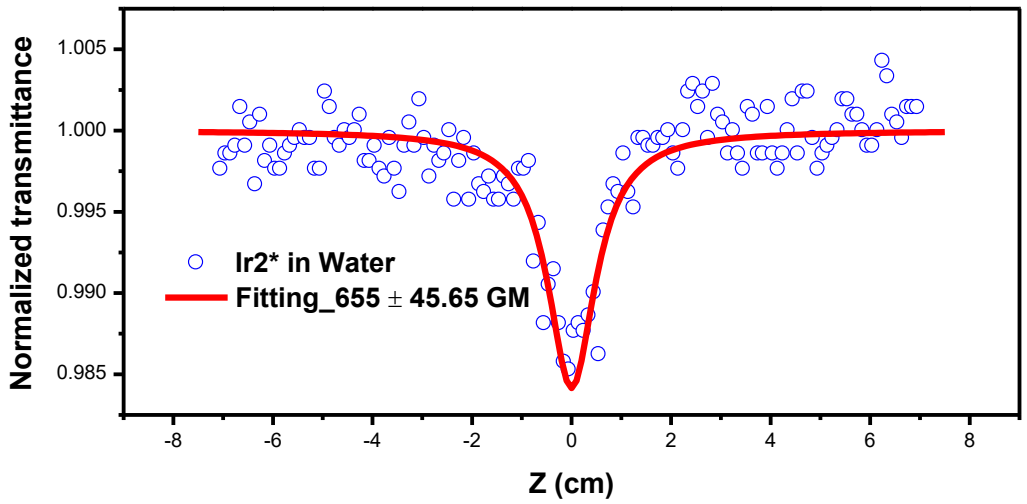
Normalized transmittance
1.005
1.000
0.995
0.990
0.985
Ir2* in Water
Fitting_655 ± 45.65 GM
-8
-6
-4
-2
0
2
4
6
8
Z (cm)

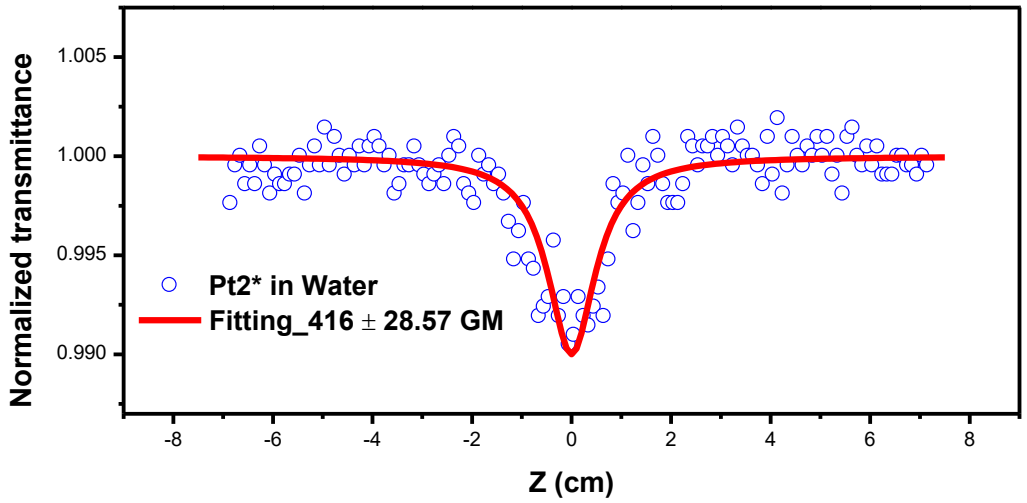
Normalized transmittance
1.005
1.000
0.995
0.990
Pt2* in Water
Fitting_416 ± 28.57 GM
-8
-6
-4
-2
0
2
4
6
8
Z (cm)

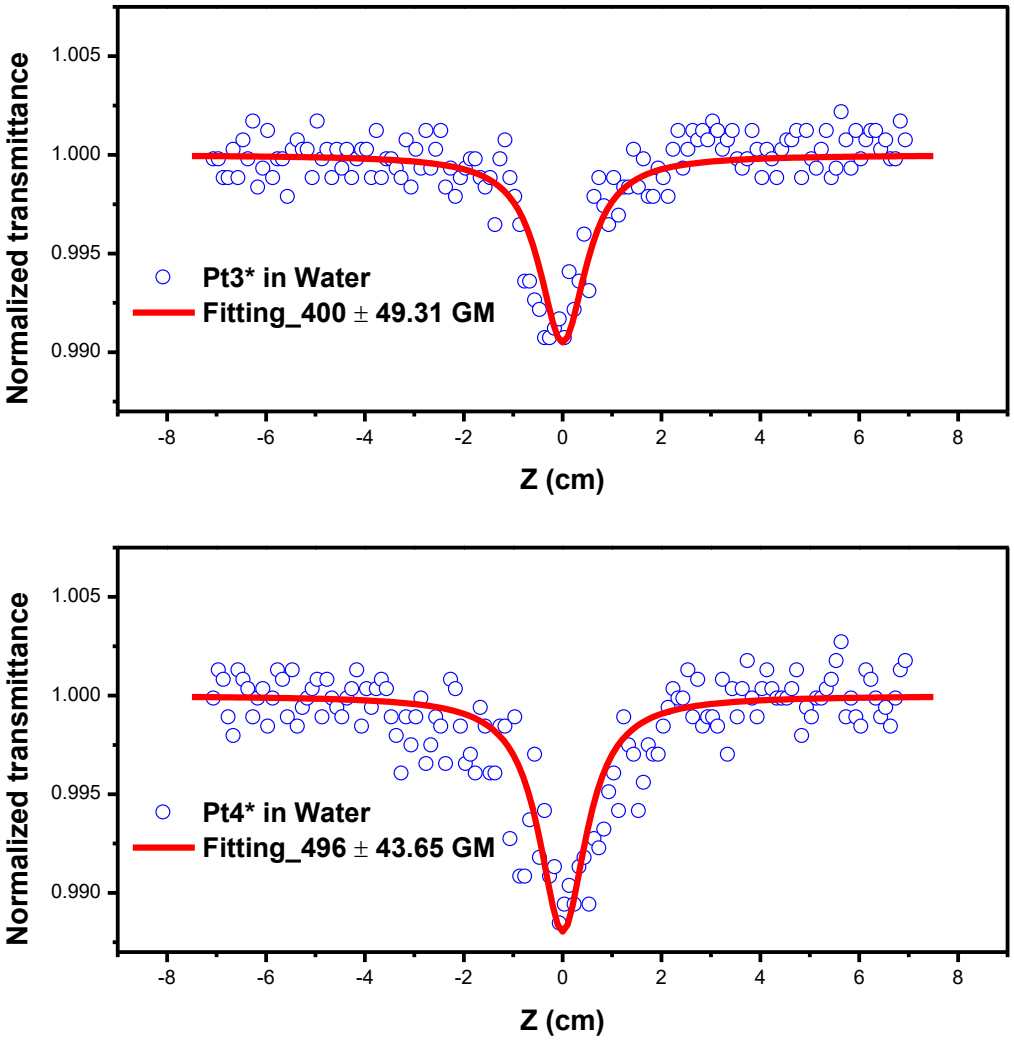

Figure S36. Open aperture Z-scan experimental results of **Ir1***, **Ir2***, **Pt2***, **Pt3***, and **Pt4*** in Water (1×10^{-4} M), obtained with 800 nm light source. Hollow circles are original experimental results, and solid line is theoretical fitting according to equation S1 and S2. Standard deviation estimated from three replicates.

Two-photon luminescence imaging

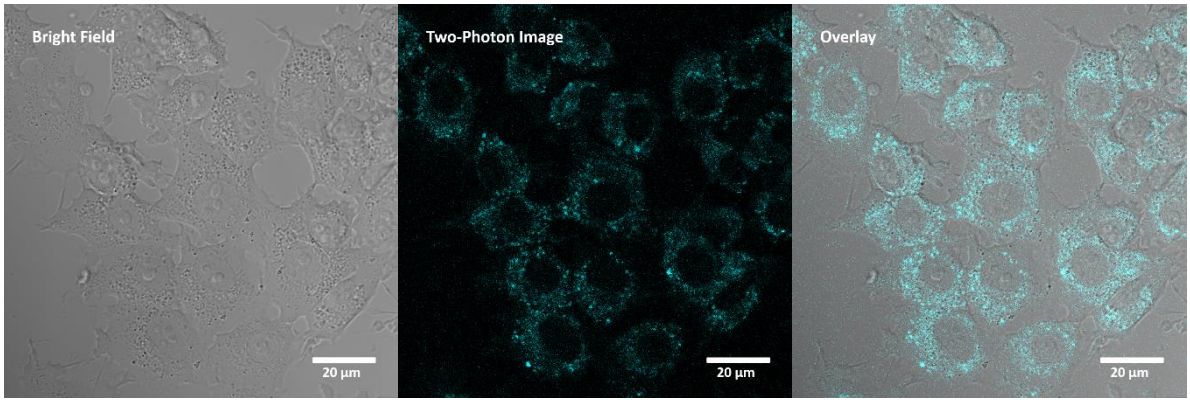

Figure S37. Two-photon image of HeLa cell labelled with **Ir1*** (50µM for 18hours). Excitation: 720 nm; Detection: 480~520nm. Scale bar: 20µm.

Ir2* (Excitation: 860 nm, Detection: 550~600 nm)

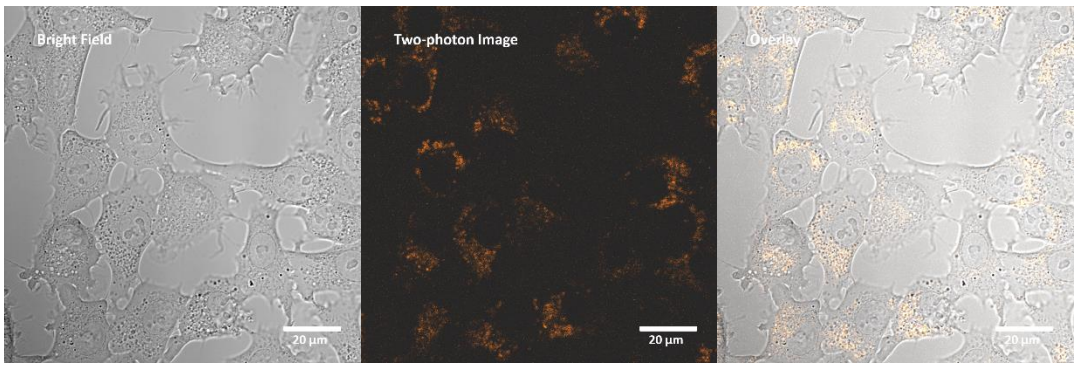

Pt2* (Excitation: 860 nm, Detection: 580~680 nm)

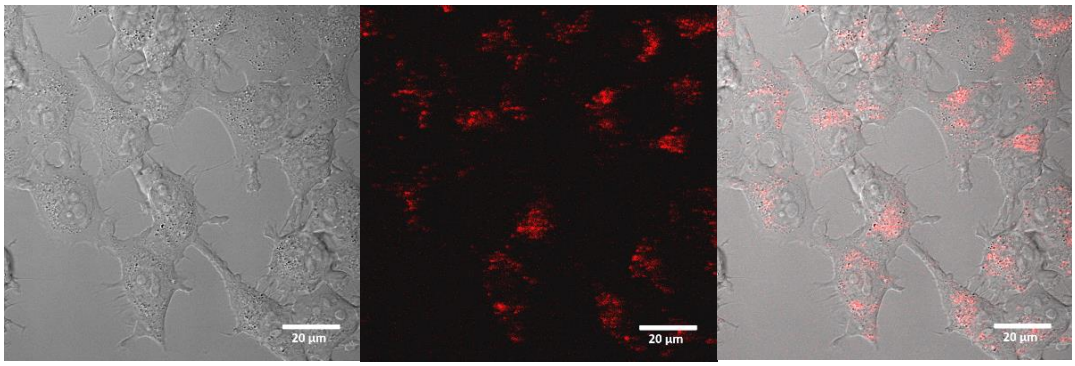

Pt3* (Excitation: 860 nm, Detection: 580~680 nm)

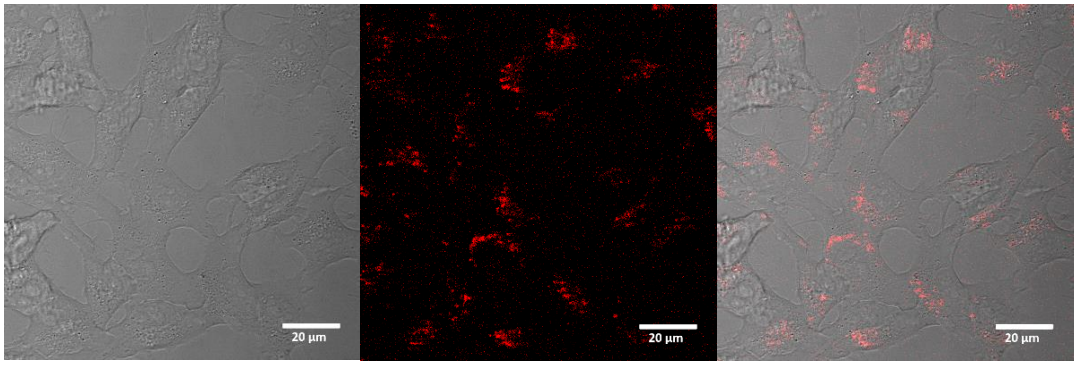

Pt4* (Excitation: 860 nm, Detection: 580~680 nm)

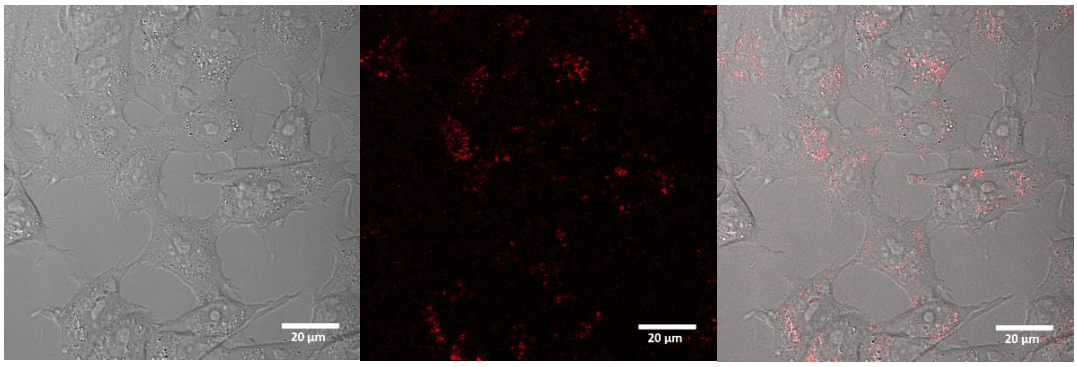

Figure S38. Two-photon image of HeLa cell labelled with **Ir2*** (50μM for 18 hours), and **Pt2*, Pt3*, Pt4*** (75μM for 18 hours). Scale bar is 20μm.

HeLa cell viability of Pt and Ir complexes

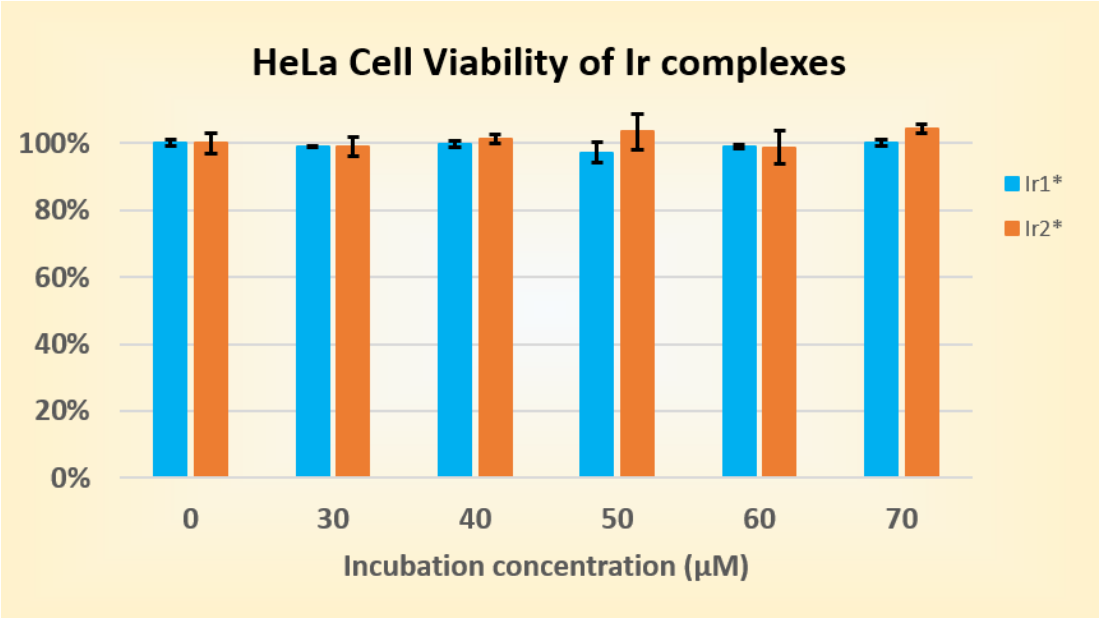

Figure S39. HeLa cell viability by MTT assay as a function of incubation concentrations of iridium complexes. Error bar represents the standard deviation calculated from three replicates.

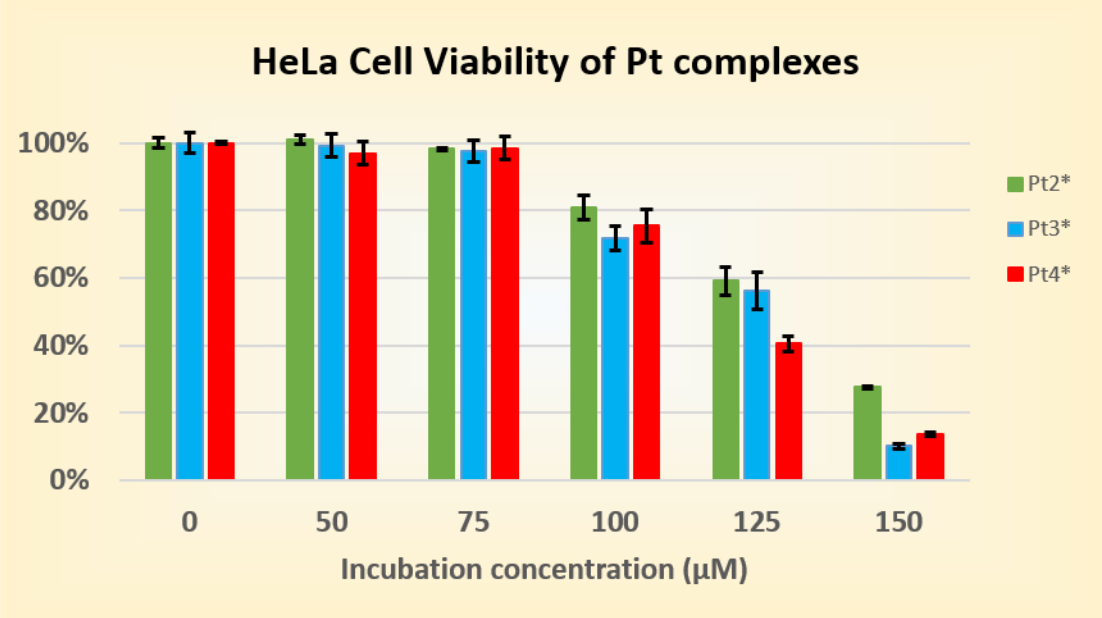

Figure S40. HeLa cell viability by MTT assay in different incubation concentration of platinum complexes. Error bar represents the standard deviation calculated from three replicates.

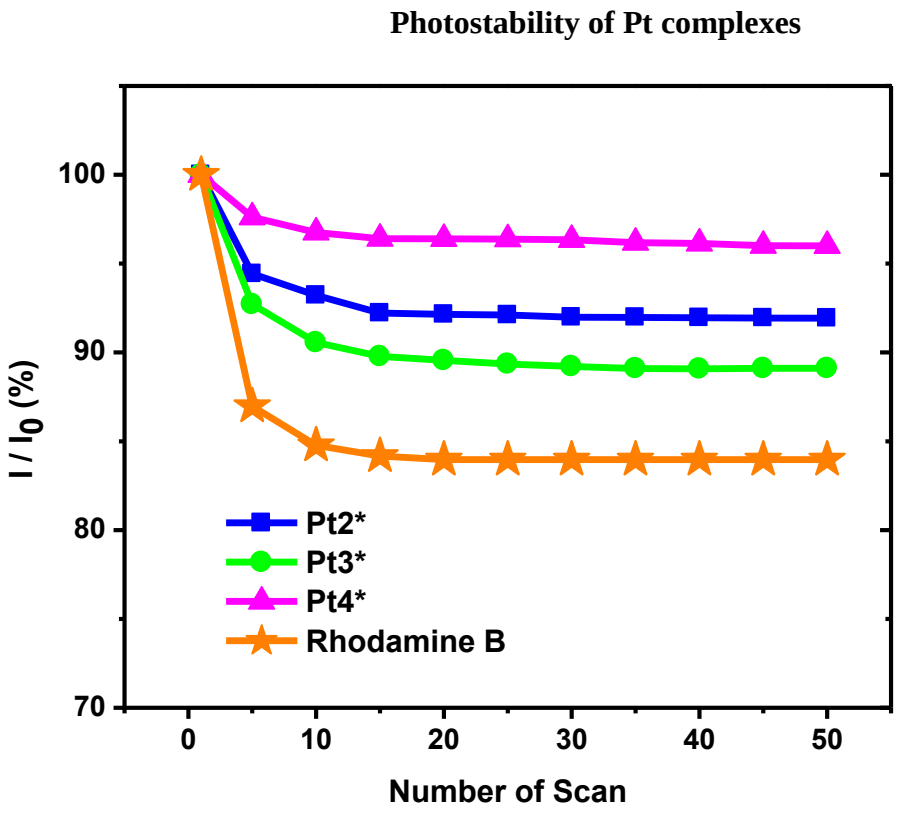

Figure S41. Photostability plot of **Pt2***, **Pt3***, **Pt4*** compared with common luminophore, Rhodamine B. Experimental Conditions: 10mM PBS buffer (pH 7.4); all the absorbances are fixed to 0.05 at 430 nm (**Pt2***, **Pt3***, **Pt4*** and Rhodamine B, λ_{exc} = 860 nm). Excitation power is controlled at 32 mW. I is the emission intensity of each particular scan, and I_0 is the emission intensity of the first scan.

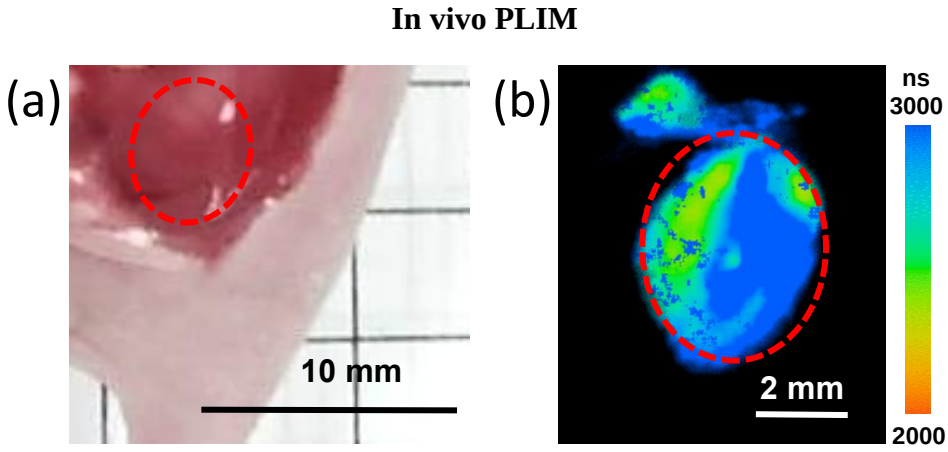

Figure S42. *In vivo* imaging of **Ir1*** phosphorescence in mouse muscle. (a) Photograph of muscle in nu/nu mouse leg with surgically opened skin flap; (b) PLIM of tumor *in vivo* after local injection of **Ir1***.

Table S4. Excited state lifetimes of **Ir1*** in water and 10% fetal bovine serum (FBS).

O_2, %	τ (ns) in water	τ (ns) in 10% FBS
0	2176	1779
5	1658	
10	1377	
15	1175	1128
20	1031	
25	913	
30	807	810

References:

[1] N. Miyaura, K. Yamada, A. Suzuki, Tetrahedron Lett. 20 (1979) 3437–3440.

[2] V. V. Sivchik, A.I. Solomatina, Y.-T. Chen, A.J. Karttunen, S.P. Tunik, P.-T. Chou, I.O. Koshevoy, Angew. Chemie Int. Ed. 54 (2015) 14057–14060.

[3] A.I. Solomatina, I.O. Aleksandrova, A.J. Karttunen, S.P. Tunik, I.O. Koshevoy, Dalt. Trans. 46 (2017) 3895–3905.

[4] R.B. Aghakhanpour, S.M. Nabavizadeh, M. Rashidi, M. Kubicki, Dalton Trans. 44 (2015) 15829–42.

[5] A. Aliprandi, D. Genovese, M. Mauro, L. De Cola, Chem. Lett. 44 (2015) 1152–1169.

[6] E.C. Constable, C.E. Housecroft, E. Schönhofer, J. Schönle, J. a. Zampese, Polyhedron 35 (2012) 154–160.

[7] S.X. Luo, L. Wei, X.H. Zhang, M.H. Lim, K.X.V. Lin, M.H.V. Yeo, W.H. Zhang, Z.P. Liu, D.J. Young, T.S.A. Hor, Organometallics 32 (2013) 2908–2917.

[8] J. Moussa, T. Cheminel, G.R. Freeman, L.-M. Chamoreau, J.A.G. Williams, H. Amouri, Dalt. Trans. 43 (2014) 8162–8165.

[9] S.S. Pasha, P. Alam, S. Dash, G. Kaur, D. Banerjee, R. Chowdhury, N. Rath, A. Roy Choudhury, I.R. Laskar, RSC Adv. 4 (2014) 50549–50553.

[10] A. Díez, J. Forniés, A. García, E. Lalinde, M.T. Moreno, Inorg. Chem. 44 (2005) 2443–53.

[11] J. DePriest, G.Y. Zheng, N. Goswami, D.M. Eichhorn, C. Woods, D.P. Rillema, Inorg. Chem. 39 (2000) 1955–1963.